PHYSICAL REVIEW D **83,** 075012 (2011)

Z' physics with early LHC data

Elena Accomando,[1,2,*] Alexander Belyaev,[1,2,†] Luca Fedeli,[3,‡] Stephen F. King,[1,§] and Claire Shepherd-Themistocleous[2,‖]

[1]*School of Physics & Astronomy, University of Southampton, Highfield, Southampton SO17 1BJ, UK*
[2]*Particle Physics Department, Rutherford Appleton Laboratory, Chilton, Didcot, Oxon OX11 0QX, UK*
[3]*INFN, 50019 Sesto F., Firenze, Italy and Department of Physics and Astrophysics, University of Florence, 50019 Sesto F., Firenze, Italy*

(Received 26 November 2010; published 14 April 2011)

We discuss the prospects for setting limits on or discovering spin-1 Z' bosons using early LHC data at 7 TeV. Our results are based on the narrow width approximation in which the leptonic Drell-Yan Z' boson production cross section only depends on the Z' boson mass together with two parameters c_u and c_d. We carefully discuss the experimental cuts that should be applied and tabulate the theoretical next-to-next-to-leading order corrections which must be included. Using these results the approach then provides a safe, convenient, and unbiased way of comparing experiment to theoretical models which avoids any built-in model-dependent assumptions. We apply the method to three classes of perturbative Z' boson benchmark models: E_6 models, left-right symmetric models, and sequential standard models. We generalize each class of model in terms of mixing angles which continuously parametrize linear combinations of pairs of generators and lead to distinctive orbits in the $c_u - c_d$ plane. We also apply this method to the strongly coupled four-site benchmark model in which two Z' bosons are predicted. By comparing the experimental limits or discovery bands to the theoretical predictions on the $c_u - c_d$ plane, we show that the LHC at 7 TeV with integrated luminosity of 500 pb^{-1} will greatly improve on current Tevatron mass limits for the benchmark models. If a Z' is discovered our results show that measurement of the mass and cross section will provide a powerful discriminator between the benchmark models using this approach.

DOI: 10.1103/PhysRevD.83.075012 PACS numbers: 12.60.Cn

I. INTRODUCTION

The end of the first decade of the millennium is an exciting time in particle physics, with the CERN LHC enjoying an extended run at 7 TeV, and the Fermilab Tevatron collecting unprecedented levels of integrated luminosity, eventually up to perhaps 10 fb^{-1}, in the race to discover the first signs of new physics beyond the standard model. Since spin-1 Z' bosons are predicted by dozens of such models, and are very easy to discover in the leptonic Drell-Yan channel, this makes them good candidates for an early discovery at the LHC. For a review see Refs. [1–3] and references therein. Furthermore, high mass Z' bosons are more likely to be discovered at the LHC than at the Tevatron [4], since energy is more important than luminosity for the discovery of high mass states. This makes the study of Z' bosons both timely and promising and has led to widespread recent interest in this subject (see for example [5–21]).

Since one of the purposes of this paper is to facilitate the connection between experiment and theory, it is worth being clear at the outset precisely what we mean by a Z' boson. To an experimentalist a Z' is a resonance ''bump'' more massive than the Z of the standard model (SM) which can be observed in Drell-Yan production followed by its decay into lepton-antilepton pairs. To a phenomenologist a Z' boson is a new massive electrically neutral, colorless boson (equal to its own antiparticle) which couples to SM matter. To a theorist it is useful to classify the Z' according to its spin, even though actually measuring its spin will require high statistics. For example, a spin-0 particle could correspond to a sneutrino in R-parity violating supersymmetric models. A spin-2 resonance could be identified as a Kaluza-Klein (KK) excited graviton in Randall-Sundrum models. However, a spin-1 Z' is by far the most common possibility usually considered, and this is what we shall mean by a Z' boson in this paper.

In this paper, then, we shall discuss electrically neutral colorless spin-1 Z' bosons, which are produced by the Drell-Yan mechanism and decay into lepton-antilepton pairs, yielding a resonance bump more massive than the Z. We shall be particularly interested in the prospects for discovering or setting limits on such Z' bosons using early LHC data. By early LHC data we mean the present 2010/11 run at the LHC at 7 TeV, which is anticipated to yield an integrated luminosity approximately of 1 fb^{-1}. Since the present LHC schedule involves a shutdown during 2012, followed by a restart in 2013, the early LHC data will provide the best information possible about Z' bosons over the next three years, so in this paper we shall focus exclusively on what can be achieved using these data, comparing the results with current Tevatron limits. In order

*e.accomando@soton.ac.uk
†a.belyaev@soton.ac.uk
‡fedeli@fi.infn.it
§king@soton.ac.uk
‖C.H.Shepherd-Themistocleous@rl.ac.uk

to enable contact to be made between early LHC experimental data and theoretical models, we advocate the narrow width approximation, in which the leptonic Drell-Yan Z' boson production cross section only depends on the Z' boson mass together with two parameters c_u and c_d [4]. Properly defined experimental information on the Z' boson cross section may then be recast as limit or discovery contours in the $c_u - c_d$ plane, with a unique contour for each value of Z' boson mass. Such experimental contours may then be confronted with the predictions of various theoretical models in the $c_u - c_d$ plane.

In order to illustrate how this formalism enables contact to be made with theoretical models, we study three classes of perturbative Z' boson benchmark models: E_6 models, generalized left-right (GLR) symmetric models, and generalized sequential models (GSM). Such perturbative benchmark gauge models are defined in terms of continuous mixing angles, in analogy to the E_6 class of models expressed through the linear combinations of T_χ and T_ψ generators associated with the extra $U(1)_\chi$ and $U(1)_\psi$ gauge groups parametrized by an angle θ. This approach is generalized to the left-right symmetric models described by the gauge group $SU(2)_L \times SU(2)_R \times U(1)_{B-L}$. In this case, the various left-right symmetric Z' models are described by linear combinations of T_{3R} and T_{B-L} generators associated with the third component of $SU(2)_R$ and to $U(1)_{B-L}$, respectively, (B and L labeling here the baryon and lepton number) parametrized by an angle ϕ.[1] Similarly, we define a new class of SM-like Z' (GSM) models based on linear combinations of T_{3L} and Q generators, associated to the third component of $SU(2)_L$ and the QED group $U(1)_Q$ respectively, with the precise linear combination in each case parameterized by a separate angle α. The strength of the parametrization we suggest is that it allows to conveniently generalize existing popular scenarios promoting them from the level of single model benchmarks to the class of the infinite set of models. On the other hand, it is important to stress that using the language of c_u-c_d variables, the whole class of the above models as well as any general model can be unambiguously presented in the $c_u - c_d$ plane as an orbit parametrized by the respective angle. We have found that the different orbits turn out to be nonoverlapping for the above mentioned three classes of models which in the following we label as $E_6(\theta)$, GLR(ϕ) and GSM(α), respectively. Although in principle all these models may originate from some high energy string inspired E_6 theory, in practice we shall regard them as independent low energy theories. In this analysis we ignore the effect of the non-SM particles on the width $\Gamma_{Z'}$. In addition we ignore the effects of $Z - Z'$ mixing since this is model dependent. However, any such mixing must be small due to the constraints from electroweak precision measurements, and we refer to such constraints on the mixing angle where possible. Working to next-to-next-leading order (NNLO) we show that the LHC at 7 TeV with as little data as $500pb - 1$ can either greatly improve on current Tevatron mass limits, or discover a Z', with a measurement of the mass and cross section providing powerful resolving power between the benchmark models using this approach. We also briefly discuss the impact of the Z' boson width on search strategies.

We also extend the method to strongly coupled models, where in principle Z' bosons could emerge from techni-rho bound states in walking technicolor models, or a series of strongly interacting resonances such as the KK excitations of the Z boson. In particular, we shall consider the strongly coupled four-site (4S) Higgsless model in which two Z' bosons are predicted [13]. Our reasons for focusing on this model are two-fold. First of all, it is representative of a class of theories which has had a major evolution in the last decade. In the past, they were described by the three-site or BESS (breaking electroweak symmetry strongly) model [22] predicting just one Z' boson constrained to be highly fermiophobic in order to satisfy both electroweak precision test (EWPT) and unitarity bounds. If this were the case, there would be no hope of evidence of these models in the Drell-Yan channel. However, in the last decade, the landscape of strongly interacting Higgsless theories has changed drastically. The new theoretical formulations, which include among others the four-site model and the minimal walking technicolor, are no longer fermiophobic. Owing to the appearance of a second extra Z' resonance, the Z' boson couplings to ordinary matter can be of the same order of magnitude as the SM ones. This opens up the possibility of revealing these particles in the favored Drell-Yan channel, during the early stage of the LHC data taking, a feature which has not been fully appreciated in the literature or in search strategies. The four-site model is therefore representative of the physics of a typical strongly interacting Z' model and by representing it for the first time in the $c_u - c_d$ plane, it is clearly seen that the associated Z' bosons may easily be distinguished from those of the perturbative gauge models.

We emphasize that in our study we made a choice of particular benchmark (classes of) models to represent different qualitative features of Z' models, such as the fact that perturbative models typically involve a single Z' boson with a relatively narrow width (which however can get larger if non-SM particles are included in the decays in addition to SM particles), while the strongly coupled models typically involve multiple Z' bosons with rather

[1]We remark that in [20] the authors focused on models obtained by taking a linear combination of the T_{B-L} generator and the hypercharge generator $Y = T_{3R} + T_{B-L}$. What they do is therefore related to the GLR models that we consider in this paper. However, the choice of generator basis and parametrization is different. They did not use the mixing angle parametrization that we propose here. Also note that in both approaches only the Abelian gauged subgroup is considered which when broken corresponds to a massive Z'.

broad widths. It is worth pointing out that these typical distinguishing features may become blurred in certain limits. For example, as already mentioned, the low energy $E_6(\theta)$, GLR(ϕ), and GSM(α) classes of models considered here may all originate from some high energy string inspired E_6 theory. Such string inspired E_6 theories may also lead to even more general classes of low energy theories containing additional Z' (and W') bosons [23].

II. BENCHMARK MODELS

A. Couplings

At collider energies, the gauge group of a typical model predicting a single extra Z' boson is

$$SU(3)_C \times SU(2)_L \times U(1)_Y \times U'(1), \tag{2.1}$$

where the standard model is augmented by an additional $U'(1)$ gauge group. The $U'(1)$ gauge group is broken near the TeV scale giving rise to a massive Z' gauge boson with couplings to a SM fermion f given by

$$\mathcal{L}_{\rm NC} = g' Z'_\mu \bar{f} \gamma^\mu (\epsilon_L^f P_L + \epsilon_R^f P_R) f, \tag{2.2}$$

where $P_{L,R} = (1 \mp \gamma_5)/2$, and $\epsilon_L^f(\epsilon_R^f)$ is the left (right) coupling between the ordinary matter and the Z' boson with $f = u, d, e, \nu_e$.

Excluding the right-handed neutrinos (which we assume to be heavier than the Z') and assuming universality amongst the three families, there are five independent couplings $\epsilon_L^{e=\nu}$, $\epsilon_L^{u=d}$, ϵ_R^u, ϵ_R^d, ϵ_R^e. In our study we prefer to work in terms of g_V^f and g_A^f which are vector and axial couplings, respectively, defined as

$$g_{V,A}^f = \epsilon_L^f \pm \epsilon_R^f. \tag{2.3}$$

In this notation $\mathcal{L}_{\rm NC}$ takes the form

$$\mathcal{L}_{\rm NC} = \frac{g'}{2} Z'_\mu \bar{f} \gamma^\mu (g_V^f - g_A^f \gamma^5) f. \tag{2.4}$$

The values of g_V^f, g_A^f depend on the particular choice of $U'(1)$. Let us stress that these eight couplings are not all independent—there are only five independent combinations of them corresponding to a number of independent ϵ_L, ϵ_R^f couplings as discussed above. Together with g' these coupling entirely encode any specific Z' model. Throughout, we follow the conventions of [1].

A slightly more complicated setup is needed to describe the four-site model which, in this paper, has been chosen to represent Higgsless multiple Z'-boson theories. The corresponding framework will be given in Sec. .

Throughout the paper we shall ignore the couplings of the Z' to non-SM particles, which all together may increase the width of the Z' by up to about a factor of 5 [24] and hence lower the branching ratio into leptons by the same factor.

B. Perturbative gauge theories

1. E_6 models

In these models one envisages that at the grand unified theory (GUT) scale the gauge group is E_6. The gauge group E_6 is broken at the GUT scale to $SO(10)$ and a $U(1)_\psi$ gauge group,

$$E_6 \to SO(10) \times U(1)_\psi. \tag{2.5}$$

The $SO(10)$ is further broken at the GUT scale to $SU(5)$ and a $U(1)_\chi$ gauge group,

$$SO(10) \to SU(5) \times U(1)_\chi. \tag{2.6}$$

Finally the $SU(5)$ is broken at the GUT scale to the SM gauge group,

$$SU(5) \to SU(3)_C \times SU(2)_L \times U(1)_Y. \tag{2.7}$$

All these breakings may occur at roughly the GUT scale. The question that concerns us here is what happens to the two Abelian gauge groups $U(1)_\psi$ and $U(1)_\chi$ with corresponding generators T_ψ and T_χ. Do they both get broken also at the GUT scale, or may one or other of them survive down to the TeV scale? In general it is possible for some linear combination of the two to survive down to the TeV scale,

$$U(1)' = \cos\theta U(1)_\chi + \sin\theta U(1)_\psi, \tag{2.8}$$

where $-\pi/2 < \theta \leq \pi/2$. More correctly, the surviving E_6 generator Q_{E_6} should be written as

$$Q_{E_6} = \cos\theta T_\chi + \sin\theta T_\psi. \tag{2.9}$$

Some popular examples of such $U(1)'$ are shown in Table I.

The resulting heavy Z' couples as $g' Q_{E_6} Z'$. Note that in E_6 models it is reasonable to assume that the Z' gauge coupling g' is equal to the GUT normalized $U(1)_Y$ gauge coupling of the SM, $g_1(M_Z) = (e/c_W)\sqrt{5/3} \approx 0.462$ where $e = 0.3122(2)$ and $c_W = \sqrt{1 - s_W^2}$ where the $\overline{\rm MS}$ value is $s_W^2 = 0.2312$. Thus, we take $g' \approx 0.46$. GUT normalization also implies that the T_ψ charges of the fermions in the $SO(10)$ 16 representation for the ψ case are all equal to $1/\sqrt{24}$, while for the χ case the T_χ charges of the $SU(5)$ representations $(10, \bar{5}, 1)$ are $(-1/\sqrt{40}, 3/\sqrt{40}, -5/\sqrt{40})$. Recalling that $g_{V,A}^f = \epsilon_L^f \pm \epsilon_R^f$, and Q, u^c, $e^c \in 10$ and L, $d^c \in \bar{5}$, and that u^c, d^c, e^c have opposite charges to u_R, d_R, e_R, this results in the values of the $g_{V,A}^f$ charges for the $U(1)_\psi$ and $U(1)_\chi$ cases as shown in Table I. The general charges as a function of θ are then simply given as

$$g_{V,A}^f(\theta) = \cos\theta g_{V,A}^f(\chi) + \sin\theta g_{V,A}^f(\psi), \tag{2.10}$$

where the numerical charges for the popular models quoted in the literature are listed in Table I.

TABLE I. Benchmark model parameters and couplings. The angles θ, ϕ, and α are defined in the text.

$U(1)'$	Parameter	g_V^u	g_A^u	g_V^d	g_A^d	g_V^e	g_A^e	g_V^ν	g_A^ν
E_6 ($g' = 0.462$)	θ								
$U(1)_\chi$	0	0	−0.316	−0.632	0.316	0.632	0.316	0.474	0.474
$U(1)_\psi$	0.5π	0	0.408	0	0.408	0	0.408	0.204	0.204
$U(1)_\eta$	-0.29π	0	−0.516	−0.387	−0.129	0.387	−0.129	0.129	0.129
$U(1)_S$	0.129π	0	−0.129	−0.581	0.452	0.581	0.452	0.516	0.516
$U(1)_I$	0.21π	0	0	0.5	−0.5	−0.5	−0.5	−0.5	−0.5
$U(1)_N$	0.42π	0	0.316	−0.158	0.474	0.158	0.474	0.316	0.316
GLR ($g' = 0.595$)	ϕ								
$U(1)_R$	0	0.5	−0.5	−0.5	0.5	−0.5	0.5	0	0
$U(1)_{B-L}$	0.5π	0.333	0	0.333	0	−1	0	−0.5	−0.5
$U(1)_{\rm LR}$	-0.128π	0.329	−0.46	−0.591	0.46	0.068	0.46	0.196	0.196
$U(1)_Y$	0.25π	0.833	−0.5	−0.167	0.5	−0.5	0.5	−0.5	−0.5
GSM ($g' = 0.760$)	α								
$U(1)_{\rm SM}$	-0.072π	0.193	0.5	−0.347	−0.5	−0.0387	−0.5	0.5	0.5
$U(1)_{T_{3L}}$	0	0.5	0.5	−0.5	−0.5	−0.5	−0.5	0.5	0.5
$U(1)_Q$	0.5π	1.333	0	−0.666	0	−2.0	0	0	0

2. Generalized left-right symmetric models

These models are motivated by the left-right (LR) extensions of the SM gauge group with the symmetry breaking,

$$SU(2)_L \times SU(2)_R \times U(1)_{B-L} \to SU(2)_L \times U(1)_Y \tag{2.11}$$

which, from the point of view of Z' models essentially involves the symmetry breaking

$$U(1)_R \times U(1)_{B-L} \to U(1)_Y, \tag{2.12}$$

where $U(1)_R$ involves the generator T_{3R} corresponding to the third component of $SU(2)_R$, while $U(1)_{B-L}$ involves the generator $T_{B-L} = (B-L)/2$. The hypercharge generator is then just given by $Y = T_{3R} + T_{B-L}$. Assuming a left-right symmetry, the resulting heavy $Z'_{\rm LR}$ couples as $g_1 Q_{\rm LR} Z'$, where

$$Q_{\rm LR} = \sqrt{\frac{3}{5}}\left(\alpha T_{3R} - \frac{1}{\alpha} T_{B-L}\right) \tag{2.13}$$

with $\alpha = \sqrt{\cot^2\theta_W - 1} \approx 1.53$ and $g_1 \approx 0.462$ as before [1].

The left-right symmetric models therefore motivate a $U(1)_{\rm LR}$ which is a particular linear combination of $U(1)_R$ and $U(1)_{B-L}$ with a specific gauge coupling. From this perspective the special cases where the Z' corresponds to a pure $U(1)_R$ or a pure $U(1)_{B-L}$ are not well motivated. Nevertheless these types of Z' have been well studied in the literature and so it is useful to propose a generalization of the LR models which includes these special cases. To this end we propose a GLR symmetric model in which the Z' corresponds to a general linear combination of the generators of $U(1)_R$ and $U(1)_{B-L}$,

$$Q_{\rm GLR} = \cos\phi T_{3R} + \sin\phi T_{B-L}, \tag{2.14}$$

where $-\pi/2 < \phi \leq \pi/2$. The gauge coupling g' is fixed so that for a particular value of ϕ the Z' of the GLR may be identified with the Z' of the LR symmetric model above. To be precise, we identify, for a particular value of ϕ:

$$g_1 Q_{\rm LR} \equiv g' Q_{\rm GLR}, \tag{2.15}$$

which implies $\tan\phi = -1/\alpha^2$ which corresponds to $\phi = -0.128\pi$ for $\alpha \approx 1.53$ and we find $g' = 0.595$. Keeping $g' = 0.595$ fixed, we are then free to vary ϕ over its range where $\phi = -0.128\pi$ gives the LR model, but other values of ϕ define new models.

Clearly $\phi = 0$ gives a $U(1)_R$ model while $\phi = \pi/2$ gives a $U(1)_{B-L}$ model. In the GLR model the value of $\phi = \pi/4$ also defines a Z' which couples to hypercharge $Y = T_{3R} + T_{B-L}$ (not to be confused with the sequential SM Z' which couples like the Z). The couplings of the Z' for the special cases of the GLR models are give in Table I. The general charges as a function of ϕ are then simply given as

$$g^f_{V,A}(\phi) = \cos\phi g^f_{V,A}(R) + \sin\phi g^f_{V,A}(B-L), \tag{2.16}$$

where the numerical charges for particular models are shown in Table I.

3. Generalized sequential models

No study is complete without including the sequential standard model (SSM) $Z'_{\rm SSM}$ which is defined to have identical couplings as for the usual Z, namely, given by $\frac{g_2}{c_W} Q_Z Z'_{\rm SSM}$ and $Q_Z = T_{3L} - s_W^2 Q$ where $s_W^2 = 0.2312$ and $\alpha_2(M_Z) = g_2^2/(4\pi) \approx 0.0338$ imply that $\frac{g_2}{c_W} \approx 0.74$. Similar to the GLR models, it is useful to define a generalized version of the SSM called GSM where the heavy

gauge boson $Z'_{\rm GSM}$ then couples as $g' Q_{\rm GSM} Z'_{\rm GSM}$, where $Q_{\rm GSM}$ corresponds to a general linear combination of the generators of $U(1)_{T_{3L}}$ and $U(1)_Q$,

$$Q_{\rm GSM} = \cos\alpha T_{3L} + \sin\alpha Q, \tag{2.17}$$

and where $-\pi/2 < \alpha \leq \pi/2$. The gauge coupling g' is fixed so that for a particular value of α the $Z'_{\rm GSM}$ of the GSM may be identified with the $Z'_{\rm SSM}$ of the SSM above. To be precise, we identify, for a particular value of α:

$$\frac{g_2}{c_W} Q_Z \equiv g' Q_{\rm GSM}. \tag{2.18}$$

This implies that the GSM reduces to the SSM case for $g' = \frac{g_2}{c_W}\sqrt{1 + s_W^4} \approx 0.76$ and $\tan\alpha = -0.23$, which corresponds to $\alpha = -0.072\pi$. Keeping $g' = 0.76$ fixed, we are then free to vary α over its range where $\phi = -0.072\pi$ gives the usual SSM, but other values of α define new models. Clearly $\alpha = 0$ gives a $U(1)_{T_{3L}}$ model while $\alpha = \pi/2$ gives a $U(1)_Q$ model.

The couplings of the Z' for the special cases of the GLR models are give in Table I. The general charges as a function of α are then simply given as

$$g^f_{V,A}(\alpha) = \cos\alpha g^f_{V,A}(L) + \sin\alpha g^f_{V,A}(Q), \tag{2.19}$$

where the numerical charges for particular models are shown Table I.

C. Strongly coupled gauge theories

Strongly interacting gauge theories provide an alternative mechanism for the electroweak symmetry breaking. The electroweak symmetry breaking is not driven by a light Higgs boson anymore, but it happens in a dynamical way. Such theories date back to decades. However, even if they predict the existence of new gauge bosons in order to delay at high energy the perturbative unitarity violation in vector-boson scattering amplitudes, they are not considered when performing searches of Z' bosons in the dilepton Drell-Yan channel. The reason is that historically the predicted new resonances must be fermiophobic in order to evade the EWPT constraints. However, in recent years, new models have been proposed that are able to satisfy the EWPT bounds without imposing such a strong condition. Both the minimal walking technicolor [25,26] and the four-site Higgsless model [13,27,28] predict extra Z' bosons with sizeable couplings to SM matter. Hence, they could be tested in the favored Drell-Yan channel at the Tevatron and during the early stage of the LHC.

The four-site Higgsless model

Higgsless models emerge naturally from local gauge theories in five dimensions. Their major outcome is delaying the unitarity violation of vector-boson scattering amplitudes to higher energies, compared to the SM without a light Higgs, by the exchange of Kaluza-Klein excitations [29]. Their common drawback is to reconcile unitarity with EWPT bounds. Within this framework, and in the attempt to solve this dichotomy, many models have been proposed [30–38].

In this paper, we consider the four-site Higgsless model [39] as representative of strongly coupled theories. This model belongs to the class of the so-called deconstructed theories [40–48], which come out from the discretization of the fifth dimension on a lattice, and are described by chiral Lagrangians with a number of gauge-group replicas equal to the number of lattice sites. The simplest version of this class of models is related to the old BESS model [22,49], a lattice with only three sites and $SU(2)_L \times SU(2) \times U(1)_Y$ gauge symmetry (for it, sometimes called three-site Higgsless model). In order to reconcile unitarity and EWPT bounds, this minimal version predicts indeed the new triplet of vector bosons to be almost fermiophobic. Hence, only diboson production, vector-boson fusion and triple gauge boson production processes can be used to test these models. All these channels require high energy and luminosity and will be proper for a future upgrade of the LHC [50–52].

In the strongly coupled scenario, the four-site Higgsless model represents a novelty in this respect [13,27,28]. Its phenomenological consequences are quite similar to those of the minimal walking technicolor [25,26]. The four-site model, based on the

$$SU(2)_L \times SU(2)_1 \times SU(2)_2 \times U(1)_Y \tag{2.20}$$

gauge symmetry, predicts two neutral and four charged extra gauge bosons, $Z_{1,2}$, and $W^{\pm}_{1,2}$, and is capable of satisfying EWPT constraints without necessarily having fermiophobic resonances. Within this framework, the more promising Drell-Yan processes become particularly relevant for the extra gauge boson search at the LHC. The four-site Higgsless model is described by four free parameters: g^e_{1V}, g^e_{2V}, M_{Z1}, M_{Z2}, that is the two vector couplings between $Z_{1,2}$ bosons and SM electrons and the two $Z_{1,2}$ masses (charged and neutral gauge bosons are degenerate).

In terms of the mass eigenstates, the Lagrangian describing the neutral current interaction is given by[2]

$$\mathcal{L}_{\rm NC} = \tfrac{1}{2}\bar{f}\gamma^\mu[(g^f_{1V} - g^f_{1A}\gamma_5)Z_{1\mu} + (g^f_{2V} - g^f_{2A}\gamma_5)Z_{2\mu}]f, \tag{2.21}$$

where $g^f_{1,2V}$, $g^f_{1,2A}$ are the vector and axial couplings of the extra $Z_{1,2}$ gauge bosons to ordinary matter. These couplings are all derived from the afore mentioned free parameters. In the above formula, we have included the g' coupling in the definition of $g^f_{1,2V}$ and $g^f_{1,2A}$.

The energy range, where the perturbative regime is still valid, is plotted in the left panel of Fig. 1 for different values of the ratio $z = M_{Z1}/M_{Z2}$. Owing to the exchange

[2]For details see [13,27].

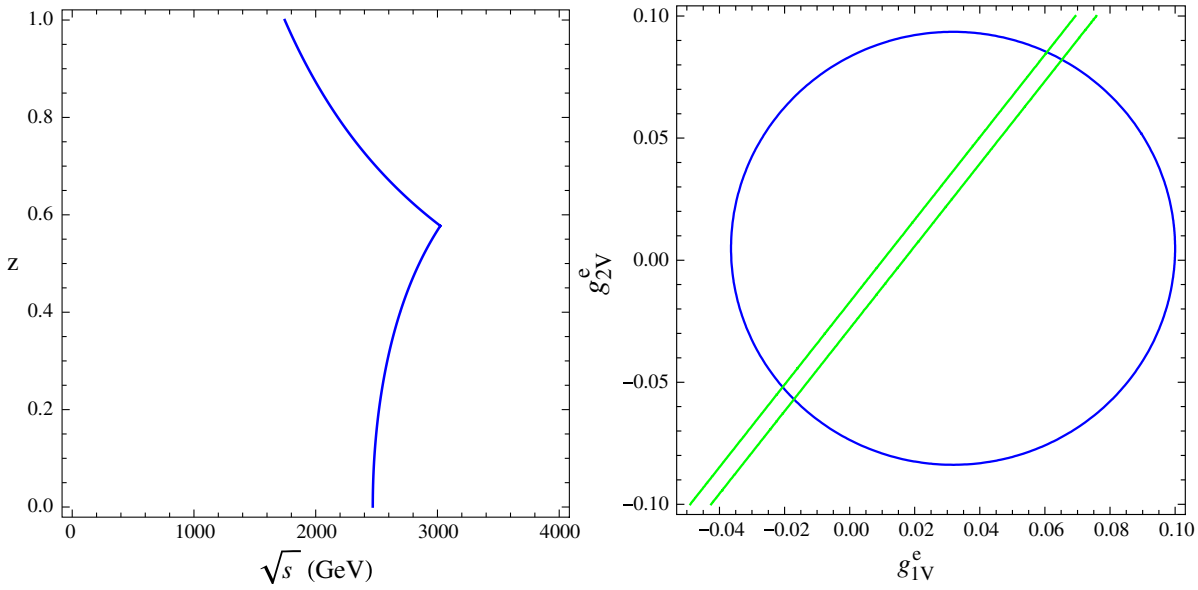

FIG. 1 (color online). Left: Unitarity bound as a function of the energy scale for different $z = M_{Z1}/M_{Z2}$ values. The perturbative region is on the left of the contour plot. Right: 95% C.L. bounds on the vector couplings of the $Z_{1,2}$ bosons to SM electrons from ϵ_1 (blue) and ϵ_3 (green). We consider the representative case: $M_{Z1} = 1$ TeV, $M_{Z2} = 1.3$ TeV.

of the extra gauge bosons, the perturbative unitarity violation can be delayed up to an energy scale of about $\sqrt{s} \simeq 3$ TeV. Hence, the mass spectrum of the new particles is constrained to be within a few TeV (see Ref. [27] and references therein for details).

In the past, the only way to combine the need of relatively low mass extra gauge bosons with EWPT was to impose the new particles to be fermiophobic. In the four-site Higgsless model, this strong assumption is not necessary anymore. In the right panel of Fig. 1, we show the bounds on the vector couplings of the $Z_{1,2}$ bosons to SM electrons coming from the EWPT expressed in terms of the $\epsilon_{1,3}$ parameters [53] (ϵ_2 is ineffective due to $SU(2)$-custodial symmetry). The outcome is that ϵ_3 constraints the relation between the two couplings, while ϵ_1 limits their magnitude (see Ref. [27] and references therein for details). As a result, one can reconcile unitarity and EWPT bounds, leaving a calculable and not fine-tuned parameter space, where the new gauge bosons are not fermiophobic.

Using the linear relation shown in the right panel of Fig. 1, we can express the Z_1-boson vector coupling to SM electrons as a function of the Z_2-boson vector coupling to SM electrons (by computing back the bare-parameters of the Lagrangian, all other $Z_{1,2}$-boson-fermion couplings can be simultaneously derived). In this way, the number of independent free parameters describing the four-site Higgsless model gets reduced to three. We choose the following physical observables: M_{Z2}, g^e_{2V}, and z. In terms of these new variables, the parameter space allowed by EWPT and perturbative unitarity is shown in Fig. 2 for one representative z value: $z = 0.8$. The outcome is that one can reconcile unitarity and EWPT bounds, leaving a calculable and not fine-tuned parameter space, where the new gauge bosons are not fermiophobic.

Compared to the popular extra $U'(1)$ theories summarized in Table I, the four-site Higgsless model does not predict fixed values for the couplings of the extra gauge

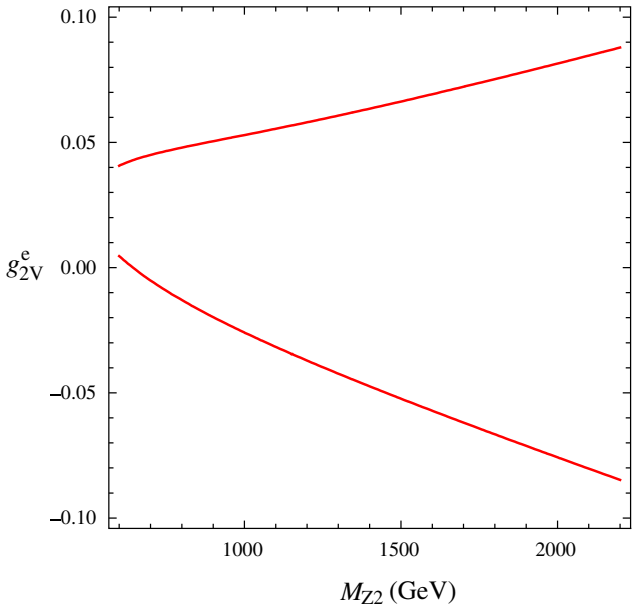

FIG. 2 (color online). Parameter space in the plane (g^e_{2V}, M_{Z2}) where g^e_{2V} is the Z_2-boson vector coupling to the SM electrons, and M_{Z2} is the Z_2-boson mass. The red solid lines restrict the area allowed by EWPT and unitarity. One sample case has been considered: $z = 0.8$.

bosons to ordinary matter. One has indeed a parameter space bounded but still large enough to accommodate rather sizeable Z_2-boson couplings to SM fermions. They can range from zero to the order of SM couplings. We use this framework in the next sections, when discussing four-site model properties and limits.

III. MODEL-INDEPENDENT APPROACH

A. Z' production and decay in the narrow width approximation

The Z' contribution to the Drell-Yan production cross section of fermion-antifermion pairs in a symmetric mass window around the Z' mass ($|M - M_{Z'}| \leq \Delta$) may be written as

$$\sigma_{f\bar{f}} = \int_{(M_{Z'}-\Delta)^2}^{(M_{Z'}+\Delta)^2} \frac{d\sigma}{dM^2}(pp \to Z' \to f\bar{f}X)dM^2. \quad (3.1)$$

In the narrow width approximation (NWA), it becomes

$$\sigma_{f\bar{f}} \approx \left(\frac{1}{3}\sum_{q=u,d}\left(\frac{dL_{q\bar{q}}}{dM^2_{Z'}}\right)\hat{\sigma}(q\bar{q} \to Z')\right) \times \mathrm{Br}(Z' \to f\bar{f}), \quad (3.2)$$

where the parton luminosities are written as $(\frac{dL_{q\bar{q}}}{dM^2_{Z'}})$, and $\hat{\sigma}(q\bar{q} \to Z')$ is the peak cross section given by

$$\hat{\sigma}(q\bar{q} \to Z') = \frac{\pi}{12} g'^2[(g_V^q)^2 + (g_A^q)^2]. \quad (3.3)$$

The branching ratio of the Z' boson into fermion-antifermion pairs is

$$\mathrm{Br}(f\bar{f}) \equiv Br(Z' \to f\bar{f}) = \frac{\Gamma(Z' \to f\bar{f})}{\Gamma_{Z'}}, \quad (3.4)$$

where $\Gamma_{Z'}$ is the total Z' width and the partial widths into a particular fermion-antifermion pair of N_c colors is given by

$$\Gamma(Z' \to f\bar{f}) = N_c \frac{g'^2}{48\pi} M_{Z'}[(g_V^f)^2 + (g_A^f)^2]. \quad (3.5)$$

Assuming only SM fermions in the final state and neglecting in first approximation their mass, one finds the total width

$$\Gamma_{Z'} = \frac{g'^2}{48\pi} M_{Z'}[9(g_V^{u2} + g_A^{u2}) + 9(g_V^{d2} + g_A^{d2}) + 3(g_V^{e2} + g_A^{e2}) + 3(g_V^{\nu 2} + g_A^{\nu 2})]. \quad (3.6)$$

Including the top quark mass, the term $9(g_V^{u2} + g_A^{u2})$ in Eq. (3.6) would be replaced by $6(g_V^{u2} + g_A^{u2})$ plus a phase space suppressed term proportional to $3(g_V^{u2} + g_A^{u2})$. However, for the Z' masses of about 600 GeV or greater, considered in this paper, the phase space suppression due to the top quark mass only leads to a correction below 3%, and the simple formula in Eq. (3.6) is sufficient.

Specializing to the charged lepton pair production cross section relevant for the first runs at the LHC, Eq. (3.2) may be written at the leading order (LO) as [4]

$$\sigma^{\mathrm{LO}}_{\ell^+\ell^-} = \frac{\pi}{48s}[c_u w_u(s, M^2_{Z'}) + c_d w_d(s, M^2_{Z'})], \quad (3.7)$$

where the coefficients c_u and c_d are given by

$$c_u = \frac{g'^2}{2}(g_V^{u2} + g_A^{u2})\mathrm{Br}(\ell^+\ell^-), \qquad c_d = \frac{g'^2}{2}(g_V^{d2} + g_A^{d2})\mathrm{Br}(\ell^+\ell^-), \quad (3.8)$$

and $w_u(s, M^2_{Z'})$ and $w_d(s, M^2_{Z'})$ are related to the parton luminosities $(\frac{dL_{u\bar{u}}}{dM^2_{Z'}})$ and $(\frac{dL_{d\bar{d}}}{dM^2_{Z'}})$ and therefore only depend on the collider energy and the Z' mass. All the model dependence of the cross section is therefore contained in the two coefficients, c_u and c_d. These parameters can be calculated from g_V^f, g_A^f, and g', assuming only SM decays of the Z' boson. The corresponding values for all considered benchmark models, which predict a single Z' boson purely decaying into SM fermions, are given in Table II.

A slight complication arises in Higgsless theories, which in the present paper are represented by the four-site model. Here in fact the two neutral extra gauge bosons, $Z_{1,2}$, decay preferably into diboson intermediate states. Their total width gets therefore two contributions:

$$\Gamma_{Z_i} = \Gamma^{f\bar{f}}_{Z_i} + \Gamma^{VV}_{Z_i}, \qquad (i = 1, 2), \quad (3.9)$$

where the two terms on the right-hand side represent the fermionic and bosonic decay, respectively. In more detail,

$$\Gamma^{f\bar{f}}_{Z_i} = \frac{1}{48\pi} M_{Z_i}[9(g_{iV}^{u2} + g_{iA}^{u2}) + 9(g_{iV}^{d2} + g_{iA}^{d2}) + 3(g_{iV}^{e2} + g_{iA}^{e2}) + 3(g_{iV}^{\nu 2} + g_{iA}^{\nu 2})], \quad (3.10)$$

$$\Gamma^{WW}_{Z_1} = \frac{1}{3\pi}\left(\frac{1}{16}\right)^2 \frac{M^3_{Z1}}{M^2_W}(1 - z^4)(1 + z^2), \quad (3.11)$$

$$\Gamma^{W_1W}_{Z_2} = \frac{1}{3\pi}\left(\frac{1}{16}\right)^2 \frac{M^3_{Z2}}{M^2_W} z^4(1 - z^2)^3[1 + 10z^2 + z^4], \quad (3.12)$$

with $i = 1, 2$, where in this case we have included the g' coupling in the definition of $g^f_{1,2V}$ and $g^f_{1,2A}$. In the above formulas, M_{Z1} and M_{Z2} are the masses of the two extra gauge bosons, $Z_{1,2}$, while z is their ratio, i.e. $z = M_{Z1}/M_{Z2}$. The direct consequence of this peculiarity is that the $Z_{1,2}$ leptonic branching ratio acquires a nontrivial dependence on the $Z_{1,2}$ boson mass, which reflects in an intrinsic mass dependence of the c_u and c_d coefficients. In addition, there is an external source of variation with mass. As all vector and axial couplings in the four-site model can be expressed in terms of the three independent free parameters (g^e_{2V}, M_{Z2}, z), c_u and c_d are completely specified by these quantities as well: $c_{u,d} = c_{u,d}(g^e_{2V}, M_{Z2}, z)$. This

TABLE II. Model predictions and current constraints. The direct limits above on the Z' mass, $M_{Z'}^{\mathrm{D}}$, are the result of the analysis performed in this paper while the best indirect limits, $M_{Z'}^{\mathrm{I}}$, come from either electroweak (e) fits or contact (c) interactions at LEP2 [2]. Note that in some cases, for example, in the sequential model, the indirect limits exceed the direct collider limits.

$U(1)'$	$\mathrm{Br}(e^+e^-)$	c_u	c_d	c_u/c_d	$\Gamma_{Z'}/M_{Z'}$	$M_{Z'}^{\mathrm{D}}$(GeV)	$M_{Z'}^{\mathrm{I}}$(GeV)	$\lvert\theta_{ZZ'}\rvert$
E_6 ($g' = 0.462$)								
$U(1)_\chi$	0.0606	6.46×10^{-4}	3.23×10^{-3}	0.2	0.0117	915	1141^e	1.6×10^{-3}
$U(1)_\psi$	0.0444	7.90×10^{-4}	7.90×10^{-4}	1	0.0053	915	481^c	1.8×10^{-3}
$U(1)_\eta$	0.0371	1.05×10^{-3}	6.59×10^{-4}	1.6	0.00636	940	434^c	4.7×10^{-3}
$U(1)_S$	0.0656	1.18×10^{-4}	3.79×10^{-3}	0.31	0.0117	847	1257^e	1.3×10^{-3}
$U(1)_I$	0.0667	0	3.55×10^{-3}	0	0.0106	795	1204^e	1.2×10^{-3}
$U(1)_N$	0.0555	5.94×10^{-4}	1.48×10^{-3}	0.40	0.00635	892	623^e	1.5×10^{-3}
GLR ($g' = 0.595$)								
$U(1)_R$	0.0476	4.21×10^{-3}	4.21×10^{-3}	1	0.0247	1065	442^e	-
$U(1)_{B-L}$	0.154	3.02×10^{-3}	3.02×10^{-3}	1	0.015	1035	-	-
$U(1)_{\mathrm{LR}}$	0.0246	1.39×10^{-3}	2.44×10^{-3}	0.57	0.0207	970	998^e	1.3×10^{-3}
$U(1)_Y$	0.125	1.04×10^{-2}	3.07×10^{-3}	3.4	0.0235	1135	-	-
SM ($g' = 0.760$)								
$U(1)_{\mathrm{SM}}$	0.0308	2.43×10^{-3}	3.13×10^{-3}	0.776	0.0297	1020	1787^c	9×10^{-4}
$U(1)_{T_{3L}}$	0.0417	6.02×10^{-3}	6.02×10^{-3}	1.00	0.045	1095	-	-
$U(1)_Q$	0.125	6.42×10^{-2}	1.60×10^{-2}	4.01	0.1225	1275	-	-

means that at fixed masses, M_{Z2} and $z = M_{Z1}/M_{Z2}$, these coefficients get constrained by the EWPT bounds acting on g_{2V}^e. As these limits vary with mass (see Fig. 2), c_u and c_d acquire this extra M_{Z2} dependence. The net result opens up a parameter space in the $c_d - c_u$ plane which will be displayed at due time.

As emphasized in [4], the $c_d - c_u$ plane parametrization is a model-independent way to create a direct correspondence between the experimental bounds on $pp(\bar{p}) \to Z' \to \ell^+\ell^-$ cross sections and the parameters of the Lagrangian. An experimental limit on $\sigma(pp(\bar{p}) \to Z' \to \ell^+\ell^-)$ for a given Z' mass gives in fact a linear relation between c_u and c_d,

$$c_u = a - bc_d, \tag{3.13}$$

where a, b can be regarded as known numbers given by

$$a = \frac{48s}{\pi}\frac{\sigma^{\mathrm{exp}}_{\ell^+\ell^-}}{w_u}, \qquad b = \frac{w_d}{w_u}, \tag{3.14}$$

where $\sigma^{\mathrm{exp}}_{\ell^+\ell^-}$ represents the 95% C.L. upper bound on the experimental Drell-Yan cross section which can be derived from observed data.

In practice, it is more convenient to use a log-log scale resulting in the limits appearing as contours for a fixed Z' mass in the $c_d - c_u$ plane. We use this representation in the next subsections.

B. Higher-order corrections

At higher-orders, the expression for the Z' production given by Eq. (3.7) strictly speaking is no longer valid. However, as it was shown in Ref. [4], the additional terms which are not proportional to c_u and c_d in Eq. (3.7) can be neglected at NNLO. Therefore, Eq. (3.7) gives a quite accurate description of the approach we are discussing here even at NNLO.

In the following, we take into account QCD NNLO effects as implemented in the WZPROD program [54–56] as a correction to the total Z' production cross section in the NWA.[3] We have adopted this package for simulating the Z' production, and have linked it to an updated set of parton density functions (PDF's). This set includes, in particular, the most recent versions of CTEQ6.6 [60,61] and MSTW08 [62] PDF's, which we use in our analysis. We can provide the complete code upon request.

The QCD NNLO Z' production cross sections are shown in Fig. 3 where we present the total $p\bar{p}(p) \to Z'$ cross section at the Tevatron and LHC at 7 TeV versus the Z' mass (see also Tables III and IV in the Appendix) obtained using CTEQ6.6 and MSTW08 PDFs are in quite a good agreement. Their difference is up to about 5% for ($M_{Z'} \geq$ 900 GeV) at the Tevatron and up to about 5% for the entire mass range considered at the LHC ($M_{Z'} \leq 2500$ GeV). The larger difference takes place at the Tevatron for $M_{Z'} \geq$ 900 GeV reaching 15% for $M_{Z'} = 1500$ GeV.

Here, we have taken as factorization scale the value $Q = M_{Z'}$. The further detailed analysis of the cross section variation with the scale is outside of the scope of the current paper.

It is also convenient to define customary NLO and NNLO K factors which can be useful for experimentalists in establishing Z' exclusion limits:

[3]We would like to note, that study of NLO effects for kinematical distributions involving leptons from Z' decay [57–59] is beyond the scope of this paper.

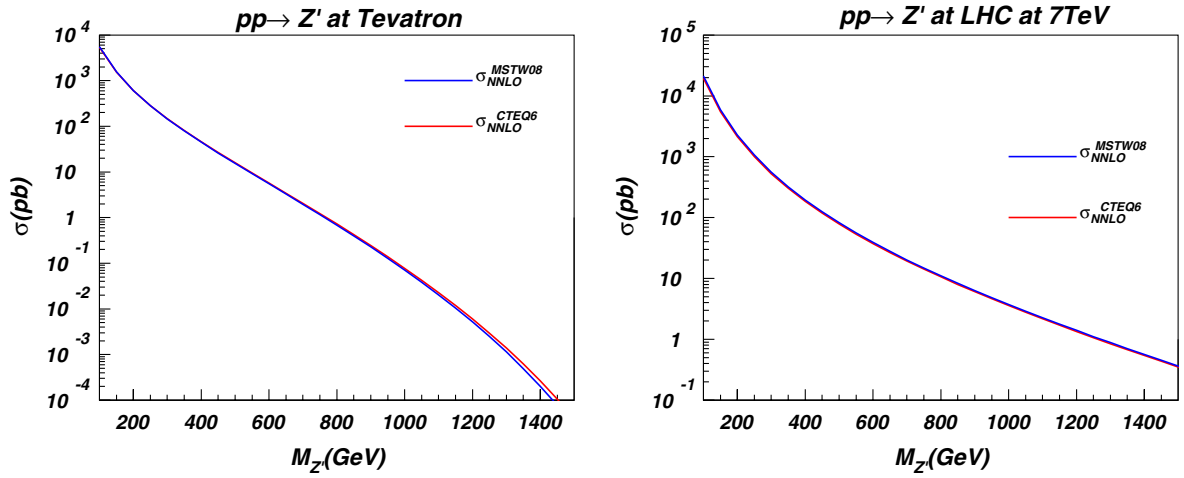

FIG. 3 (color online). $\sigma(p\bar{p}(p) \to Z')_{\mathrm{NNLO}}$ for standard model-like Z' production at the Tevatron (left panel) and the LHC at 7 TeV (right panel) for CTEQ6.6 and MSTW08 PDF's.

$$\frac{K_i = \sigma(pp(\bar{p}) \to Z')_i}{\sigma(pp(\bar{p}) \to Z')_0}, \tag{3.15}$$

where the index $i = 1, 2$ corresponds to NLO and NNLO K factors, respectively. As an example, in Fig. 4 we present the values of these K_i factors for standard model-like Z' production at the Tevatron (left panel) and the LHC at 7 TeV (right panel) for CTEQ6.6 and MSTW08 PDF's.

In contrast to the case of the NNLO Z' production cross section, where the agreement between CTEQ6.6 and MSTW08 PDF predictions is within the estimated $O(5\%)$ PDF error bands for quark initiated processes (except the high mass region at the Tevatron), there is a noticeable difference in the K_{NLO} and K_{NNLO} factors as a function of the Z' mass for CTEQ6.6 as compared to the MSTW08 PDF's. This difference is related to the way of fitting the LO PDF's of CTEQ and MSTW collaborations (see e.g. [62,63]). Furthermore, both $K^{\mathrm{MSTW08}}_{\mathrm{NLO,NNLO}}$ and $K^{\mathrm{CTEQ6}}_{\mathrm{NLO,NNLO}}$ factors display a strong dependence on the Z' mass. As an example, $K^{\mathrm{CTEQ6}}_{\mathrm{NNLO}}$ varies between 10–40% at the Tevatron and 10–30% at the LHC at 7 TeV for potentially accessible Z' masses.

Applying a universal K factor can be highly misleading. As shown above, the $K_{\mathrm{NLO,NNLO}}$ factor has indeed a two-fold source of dependence: PDF set and energy scale (i.e. $M_{Z'}$). A uniform setup must be fixed when comparing experimental limits on different models.

Since Eq. (3.7) gives an accurate description even at NNLO [4], and noting that QCD NNLO corrections are universal for up- and down-quarks, one can effectively apply the same K_{NNLO} factor derived for SM-like Z' to generic Z' models without loosing of generality. Owing to the remarkable Z' mass dependence of the K_{NNLO} factor, we first convolute the LO Z' production cross section with

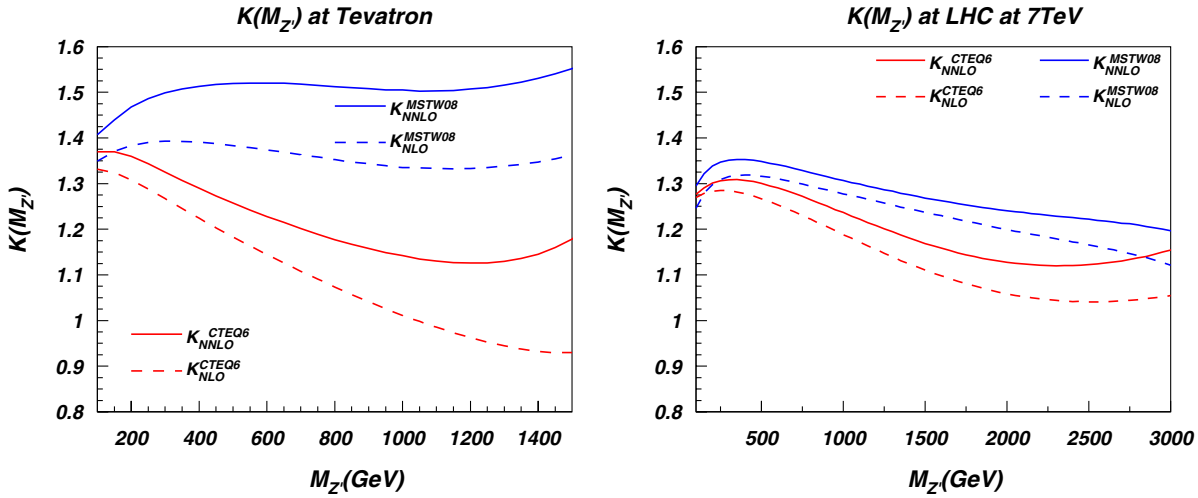

FIG. 4 (color online). NNLO and NLO K factors defined by Eq. (3.15) for standard model-like Z' production at the Tevatron (left panel) and the LHC at 7 TeV (right panel).

the respective LO PDF's and then we multiply it by $K_{\mathrm{NNLO}}(M_{Z'})$.

For convenience and clarity, we provide the values of K_{NNLO} factors and cross sections for the SM-like Z'-boson production process at the Tevatron and the LHC at 7 TeV: $p\bar{p}(p) \to Z' + X$ in Tables III and IV, shown in Appendix . The first table contains the results obtained with MSTW08 PDF, the latter with CTEQ6.6 PDF. The quoted numbers correspond to the curves visualized in Figs. 3 and 4.

In narrow width approximation, the two-fermion cross section is the product of the production cross section and the respective branching ratio. When considering the complete Z'-boson production and decay in the Drell-Yan channel, one has to keep in mind that QCD NNLO corrections also affect the Z' branching ratio even for purely leptonic decays, $\mathrm{Br}(Z' \to \ell^+\ell^-)$, since the Z' total decay width will be corrected at NNLO. This reflects into an higher order correction to the c_u and c_d coefficients, through $\mathrm{Br}(Z' \to \ell^+\ell^-)$ which explicitly enters the expression for c_u and c_d given in Eq. (3.8). The NNLO Drell-Yan cross section can be thus written as

$$\begin{aligned}\sigma^{\mathrm{NNLO}}_{\ell^+\ell^-} &= \frac{\pi}{48s}[c_u^{\mathrm{NNLO}} w_u(s, M^2_{Z'})^{\mathrm{NNLO}} + c_d^{\mathrm{NNLO}} w_d(s, M^2_{Z'})^{\mathrm{NNLO}}] \\ &\approx K^{\mathrm{PDF}}_{\mathrm{NNLO}} K^{\mathrm{BR}}_{\mathrm{NNLO}} \frac{\pi}{48s}[c_u w_u(s, M^2_{Z'}) + c_d w_d(s, M^2_{Z'})] \\ &= K^{\mathrm{PDF}}_{\mathrm{NNLO}} K^{\mathrm{BR}}_{\mathrm{NNLO}} \sigma^{\mathrm{LO}}_{\ell^+\ell^-}. \end{aligned} \tag{3.16}$$

The factorization $K^{\mathrm{PDF}}_{\mathrm{NNLO}} K^{\mathrm{BR}}_{\mathrm{NNLO}}$ in Eq. (3.16) is quite accurate bearing in mind that the factor $K^{\mathrm{BR}}_{\mathrm{NNLO}}$ is equal to unity to an accuracy of about 1–2% as discussed below. The leading NLO QCD correction to the total Z' width is known to be α_s/π [64,65]. This gives an enhancement of the order of 2–3% to the Z' width for $M_{Z'}$ in the range 500–2000 GeV. The $Br(Z' \to \ell^+\ell^-)$ will thus decrease accordingly by (2–3%) $\times$ $\mathrm{Br}(Z' \to \mathrm{hadrons})$. The net result corresponds to a 1–2% depletion of the leptonic branching ratio within the SM-like Z' model. An effect of the same order is expected for the other classes of Z' models under consideration. In the current study, we neglect this effect and use the following formula for establishing limits on Z' models:

$$\sigma^{\mathrm{NNLO}}_{\ell^+\ell^-} \simeq K^{\mathrm{PDF}}_{\mathrm{NNLO}} \sigma^{\mathrm{LO}}_{\ell^+\ell^-}. \tag{3.17}$$

Hereafter we are using the NNLO cross sections that we have calculated to estimate present and future collider limits. The study of kinematic distributions, interference effects as well as effects of invariant mass cuts which are the subject of the next section is performed at LO level. This level of approximation is quite sufficient either because the *shape* of invariant mass distribution is not visibly affected by NNLO or because the NNLO effects are essentially cancelled in the ratio of LO properties.

C. Finite width effects

So far we have discussed the Z' boson production using narrow width approximation. However, the experimental search for an extra Z' boson and the discrimination of the SM backgrounds could strongly depend on the realistic Z' width. Moreover the theoretical prediction of the Z' production cross section also depends on its width as we discuss below.

We start this discussion with Fig. 5 where we present the dilepton invariant mass distribution for the Z' boson production at LO within various models at the Tevatron (left panel) and the LHC at 7 TeV (right panel).

We consider three representative models: the SM-like Z' model (black line), the N-type E_6 model defined in Table I (red line), and the weakly coupled SM-like Z' model where the Z' boson gauge coupling to SM fermions is reduced by a factor of 10 (blue line). From top to bottom, the last two

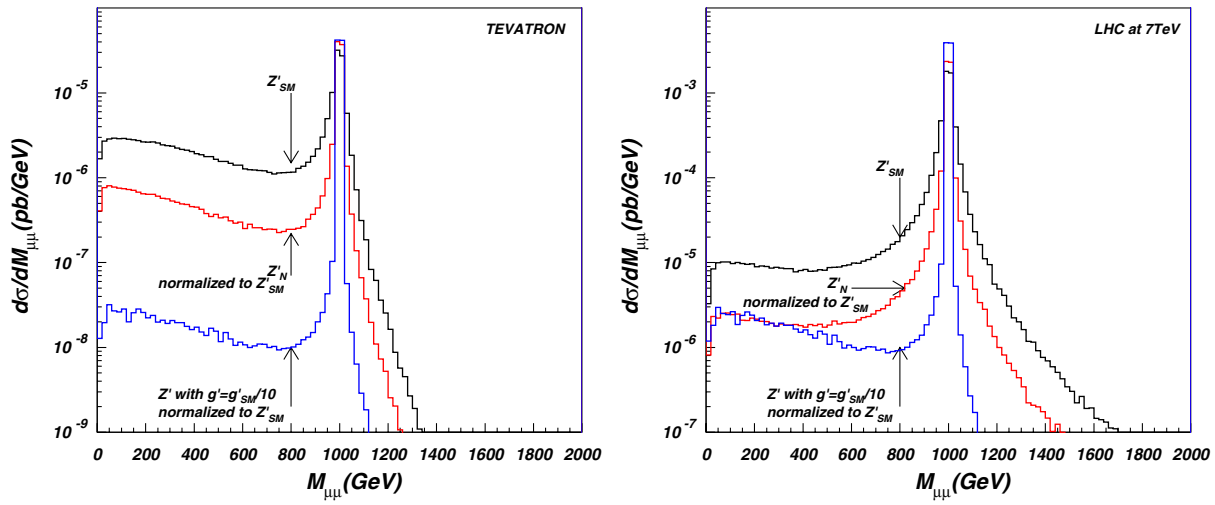

FIG. 5 (color online). Dilepton invariant mass distribution for the Z' boson production at LO in various models at the Tevatron (left panel) and LHC at 7 TeV (right panel). We consider the case: $M_{Z'} = 1000$ GeV.

distributions are normalized to the integral under the first one.

We first consider the SM-like Z' model distribution at the Tevatron. It is important to stress that the total cross section of $p\bar{p} \to Z' \to \ell^+\ell^-$ process integrated over the entire $M_{\ell^+\ell^-}$ range is almost as twice as large as the SM-like Z' in the narrow width approximation. The main reason for this effect is the specific shape of the $M_{\ell^+\ell^-}$ distribution in the region of small $M_{\ell^+\ell^-}$ far away from $M_{Z'}$. This region is exhibited by a non-negligible tail due to the steeply rising PDF in the region of low $M_{\ell^+\ell^-}$ even though the Z' boson is extremely far off mass-shell in this region. The integral over this region can even double the cross section evaluated in the NWA in the case of Z' production at the Tevatron.

This effect, which is related to the off shellness of the extra gauge boson, varies according to the total Z' width. In the Z'_N model, it brings an additional 20% contribution to the narrow width approximation cross section at the Tevatron. In the weakly coupled SM-like Z' model, the far off-shellness effects are effectively negligible (below 1%).

We can see that in general experimental limits would and should strongly depend on the particular Z' model predicting a specific Z' width. On the other hand, if one requires a dilepton mass window cut around the Z' mass, one can establish a quasi model-independent experimental upper limit on $\sigma(p\bar{p} \to Z' \times \mathrm{Br}(Z' \to \ell^+\ell^-)$ versus $M_{Z'}$ and apply this limit to constraint different classes of models.

In Fig. 6 we present the effect of a symmetric mass window cut around $M_{Z'}$ for the SM-like Z' model and two other representative models (see Table I) at the Tevatron and the LHC at 7 TeV. We fix the Z' mass to be $M_{Z'} = 1$ TeV. We show the relative difference between the full cross section for the process $pp(\bar{p}) \to Z' \to \ell^+\ell^-$ evaluated taking into account the finite Z' width (σ) and the cross section computed in narrow width approximation (σ^{NWA}). The relative difference is presented as a function if the $\Delta M/M_{Z'}$ symmetric mass window cut ($|M_{\ell^+\ell^-} - M_{Z'}| < \Delta M$) applied to the full cross section σ. One can see that for the SM-like Z' model at the Tevatron, a $\Delta M/M$ cut in the 9–25% range brings the agreement between σ and σ^{NWA} down to the 5% level, while $\Delta M/M \simeq 15\%$ exactly matches σ and σ^{NWA}. At the LHC, the corresponding range of the $\Delta M/M$ cut is 15–80%, and σ and σ^{NWA} are matched for $\Delta M/M \simeq 45\%$. The ψ model Z' has a narrower width, making the choice of the cut more insensitive, while the Q model Z' width is broader leading to a more sensitive choice of the mass window cut to reproduce the narrow width approximation. Note that all lines cross the abscissa at about the same value of $\Delta M/M_{Z'}$, meaning that there will be an optimal mass window cut consistent with all models. Note that the ψ, SSM, and Q models in Fig. 6 represent a wide range of values of c_u and c_d.

The choice of the mass window cut to gain agreement with the narrow width approximation also depends on $M_{Z'}$. This dependence is defined by proton parton densities and is therefore model independent. The net effect is again to make all the lines cross the abscissa at about the same value of $\Delta M/M_{Z'}$, where this point depends on $M_{Z'}$. Therefore, for every given mass one can work out a quasi model-independent mass window cut where the full cross section matches the narrow width approximation. The additional advantage of this choice is that in the selected mass window around the Z' mass the model-dependent interference effect between the Z' signal and SM background is highly suppressed.

The experimental limits would be quasi model independent if one would apply this cut on the $M_{\ell^+\ell^-}$ around the

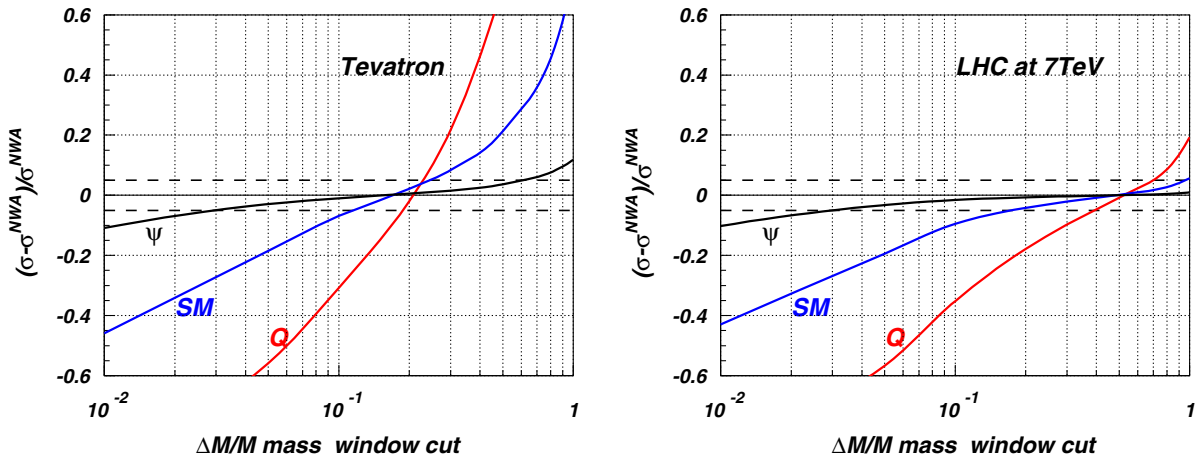

FIG. 6 (color online). Relative difference between the full cross section for $pp(\bar{p}) \to Z' \to \ell^+\ell^-$ evaluated taking into account the finite Z' width (σ) and the cross section computed in narrow width approximation (σ^{NWA}). The relative difference is presented as a function of the $\Delta M/M_{Z'}$ symmetric mass window cut $|M_{\ell^+\ell^-} - M_{Z'}| < \Delta M$ applied to the full cross section (σ). Three different representative models are considered for $M_{Z'} = 1$ TeV (see Table I).

M'_Z: it brings into agreement the cross section calculated in the narrow width approximation and in the finite width approximation as well as removes the model-dependent shape of the $M_{\ell^+\ell^-}$ distributions in the region of low $M_{\ell^+\ell^-}$, especially for the case of large Z' width effects as, for example, take place for SM-like Z'. Moreover, the cut on $M_{\ell^+\ell^-}$ around the M'_Z plays an important role in reducing an effect of Z' interference with Z/γ down to the few percent level, which again, allows to establish and use experimental limits in model-independent way.

For example, in the case of SM-like Z' production at the Tevatron, the relative interference, which is defined as $R_i = [\sigma(p\bar{p} \to Z'/Z/\gamma \to \ell^+\ell^-) - \sigma(p\bar{p} \to Z' \to \ell^+\ell^-) - \sigma(p\bar{p} \to Z/\gamma \to \ell^+\ell^-)]/\sigma(p\bar{p} \to Z' \to \ell^+\ell^-)$, is as large as about -19 (meaning -1900% of interference) for $M_{\ell^+\ell^-} > 100$ GeV cut but it drops down to -6% for the $|M_{\ell^+\ell^-} - M_{Z'}| < 0.15 M_{Z'}$ cut, which matches NWA and finite width cross sections. The effect of the mass window cuts is also quite large for the case of SM-like Z' production at the LHC, where interference is about -300% for $M_{\ell^+\ell^-} > 100$ GeV cut and only about -2% for $|M_{\ell^+\ell^-} - M_{Z'}| < 0.15 M_{Z'}$ cut.

We can see, that there is a strong motivation to use an invariant mass window cut for conducting a model-independent analysis. The size of this cut, if one aims to match the NWA and finite width cross sections, is collider dependent: it is about 15% of $M_{Z'}$ for the Tevatron and about 40% of $M_{Z'}$ for the LHC at 7 TeV.

In this paper we are using results of experimental analysis which are based on the $M_{\ell^+\ell^-}$ mass window cut similar to what we are advocating. This would allow us to use precise NNLO model predictions and perform a respective model-independent interpretation of the experimental limits.

IV. APPLICATION OF THE MODEL-INDEPENDENT APPROACH TO THE BENCHMARK MODELS

A. Current limits from Tevatron

As discussed above, collider limits on the Z'-boson mass can be presented via contours in the $c_u - c_d$ plane, with every contour corresponding to a well-defined $M_{Z'}$. Simultaneously, in the same plane, one can also show the values of the $c_{d,u}$ couplings allowed by a specific Z' model. As a result, one can immediately visualize and derive a mass bound on the Z' boson predicted by that particular model. The results for the direct limits we obtain are summarized in Table II, where other properties of particular benchmark models (such as the widths) are also displayed.

We start by presenting our results at the Tevatron, which is running at $\sqrt{s} = 1.96$ TeV. We use the most recent 95% C.L. upper bound on $\sigma(p\bar{p} \to Z' \to \ell^+\ell^-)$ reported at the ICHEP 2010 Conference by the D0 Collaboration for the dielectron channel [66,67], where the $\Delta M/M_{Z'} \simeq 15\%$ cut was used in the analysis. This limit is shown in Fig. 7 (left panel), together with its "translation" into the $c_u - c_d$ plane for different $M_{Z'}$ masses as shown in Fig. 7 (right panel). Note that D0 upper limit on the Z' cross section has been extrapolated to higher masses in the Fig. 7 (right panel). Such an extrapolation is necessary since the SM-like Z' model (SSM) does not represent the benchmark model for which the discovery/exclusion value of the Z' mass is maximal. The extrapolation was done using the fact that the expected background for large $M_{Z'}$ is close to zero, so the experimental limit on the signal rate becomes independent of $M_{Z'}$ and reaches a horizontal plateau.

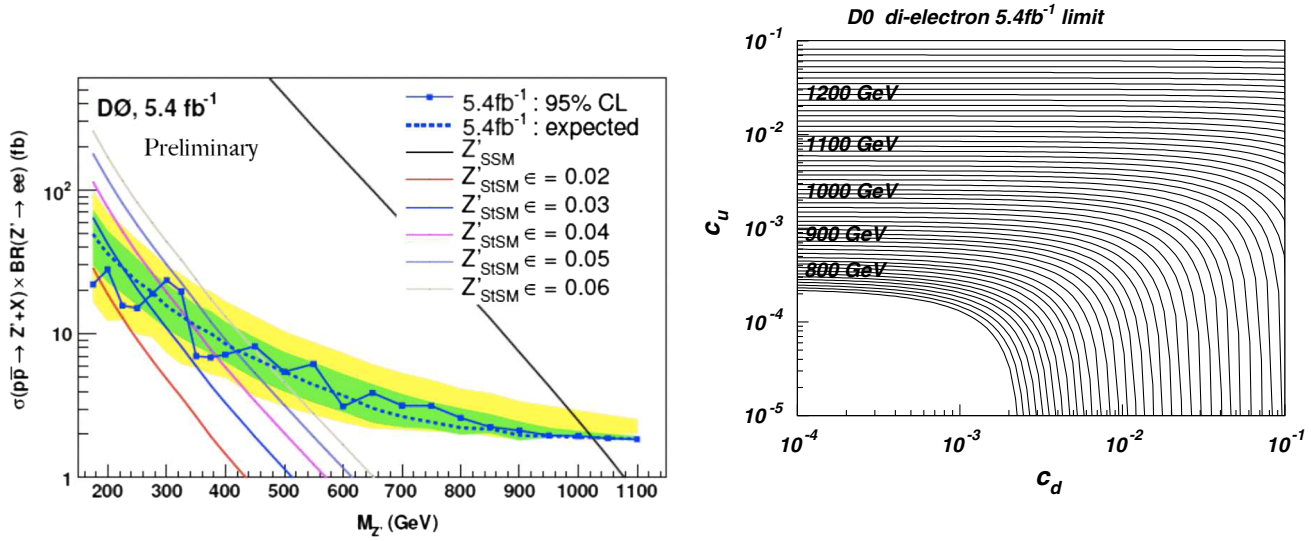

FIG. 7 (color online). Left: 95% C.L. upper bound on $\sigma(p\bar{p} \to Z' \to e^+e^-)$ obtained at the Tevatron with integrated luminosity $L = 5.4$ fb^{-1} by the D0 Collaboration [66,67]. Also shown, Z' mass bounds within the extra $U(1)'$ models displayed in the legend. Right: same 95% C.L. upper bound on $\sigma(p\bar{p} \to Z' \to e^+e^-)$ as above, but translated in the $c_u - c_d$ plane into contours corresponding to different $M_{Z'}$ masses. The low mass models refer to the Stueckelberg extensions of the SM discussed in [71,72].

In the following, we use Fig. 7 (right panel) to interpret the current limits from Tevatron, and to derive the mass bounds on the Z' boson predicted in the classes of models described in the previous section. The results are shown in Fig. 8. The top-left panel displays the contour representing E_6 models in the $c_u - c_d$ plane, the top-right panel shows the GLR, the bottom-left panel contains the GSM, and finally the bottom-right one gives the 4S Higgsless model In the first three mentioned panels, the color code corresponds to four equidistant intervals for the mixing angle in the $[-\pi/2, \pi/2]$ range for the E_6, GLR, and GSM models, represented by continuous and closed contours. The black dots on these contours denote the popular benchmark models quoted in Table I. In the bottom-right panel, which shows the parameter space of the four-site model, the color indicates different mass values for M_{Z_1} and M_{Z_2}. The line style distinguishes the Z_1 mass (solid line) from the Z_2 mass (dashed line). For the Z_1 boson, the following mass values have been chosen: $M_{Z1} = 480$ (red), 800 (green), and 1600 (blue) GeV. For the chosen sample of free parameters, $z = 0.8$, the corresponding values for the Z_2 bosons are: $M_{Z2} = 600$, 1000 and 2000 GeV shown with the same color coding.

Several comments are in order. The first remarkable fact is that there is almost no overlap between contours for the E_6, GLR, and GSM models. This means that, if a Z' boson is discovered and its cross section is measured with reasonable accuracy, these classes of Z' models can be well

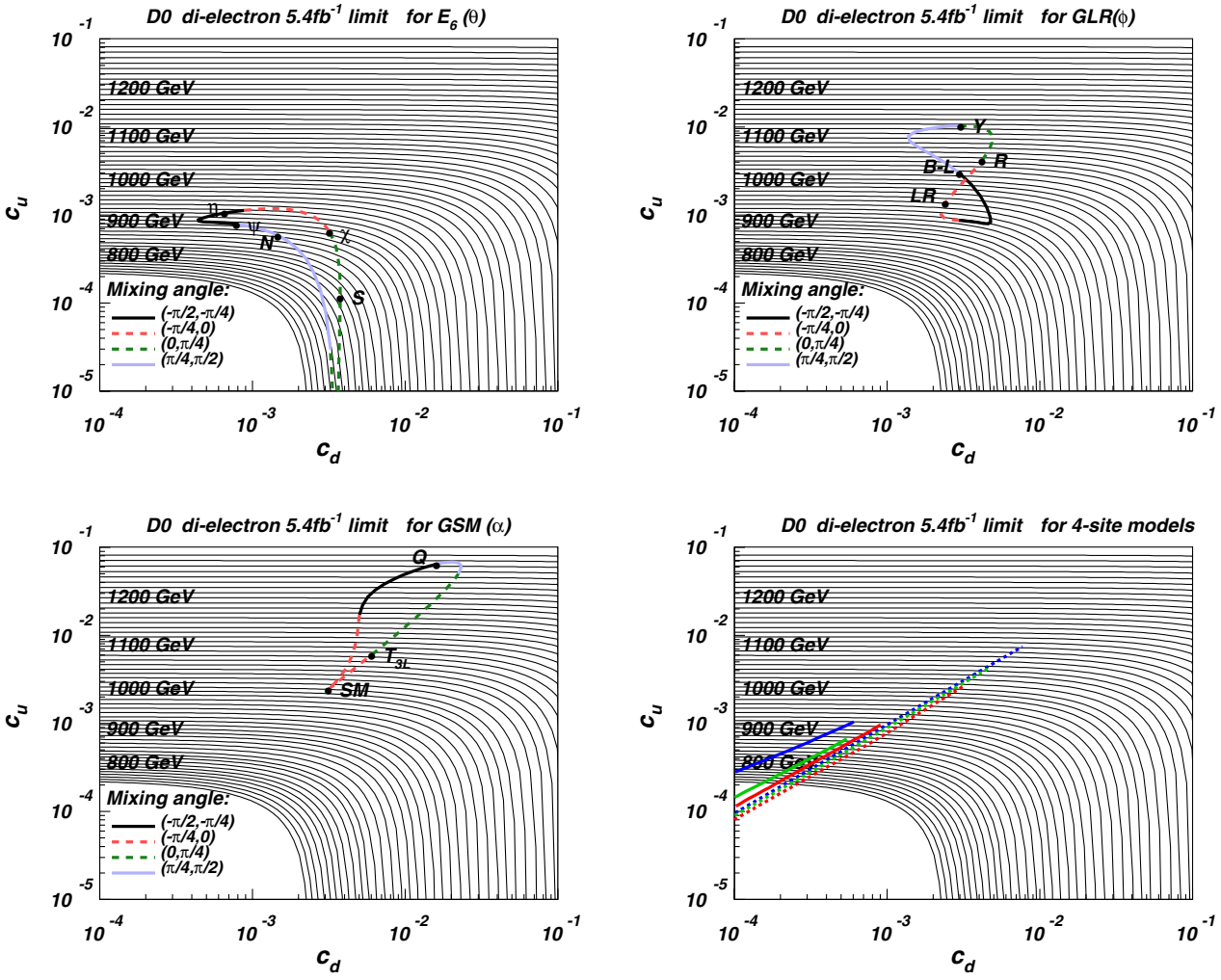

FIG. 8 (color online). 95% C.L. limits on $M_{Z'}$ in the $c_u - c_d$ plane based on the 2010 analysis of the dielectron channel performed by the D0 Collaboration at $L = 5.4$ fb^{-1}. The top-left, top-right, bottom-left, bottom-right panels present results for E_6 Models, GLR), GSM, and four-site Higgsless model, respectively. The color code corresponds to four equidistant intervals for the mixing angle within the $[-\pi/2, \pi/2]$ range for the E_6, GLR, and GSM models. The black dots on these contours correspond to the benchmark models listed in Table I. For the 4S model, the color denotes different values for M_{Z_1} and M_{Z_2}. The line style distinguishes the Z_1 mass (solid line) from the Z_2 mass (dashed line). For the Z_1 boson, the following mass values have been chosen: $M_{Z1} = 480$ (red), 800 (green) and 1600 (blue) GeV. For the chosen sample of free parameters, $z = 0.8$, the corresponding values for the Z_2 bosons are $M_{Z2} = 600$, 1000 and 2000 GeV shown with the same color coding.

distinguished using just this basic information. The second remark concerns the experimental sensitivity (i.e. ability of a given experiment to exclude or discover a Z' for a given model) to the Z' production within different models. Comparing the four plots, it is clear that the highest sensitivity is to the GSM class of models. In particular, the Q model can be excluded at the Tevatron up to masses $M_{Z'} \geq 1260$ GeV. Among the GLR models, which are second in terms of the experimental sensitivity to a Z' boson, the Y model can be already excluded up to $M_{Z'} \geq 1125$ GeV with the current Tevatron data. Interestingly, the lowest experimental sensitivity is to the E_6 class of models, which represents one of the most popular classes of Z' models. Within this class, the strongest limit can be derived for $\theta \in [-\pi/4, 0]$ providing the mass bound $M_{Z'} \geq 955$, as one can read from the red-colored part of the E_6 contour.

The 4S class of Z' models must be considered separately. First of all, it predicts two Z' bosons with two different masses. Secondly, the parameter space of the 4S model is described by more than just one parameter, so the model would be represented by an area in the $c_u - c_d$ plane rather than by a contour. In order to interpret Fig. 8 (bottom-right panel) and correctly following the analogous figures, a clarification is needed. In the 4S model, the two extra gauge bosons can decay into both SM fermion pairs and boson pairs. While the contribution to the total width coming from the decay into fermion pairs is linear in the extra gauge boson mass, the contribution from the diboson decay grows with the third power of the extra gauge boson mass [see Eq. (3.5)]. As a consequence, and opposite to the other perturbative gauge models, the $Z_{1,2}$ boson branching ratio into lepton pairs acquires a mass dependence (see Sec. III A for details). This reflects into a mass dependence of the c_u and c_d parameters which parametrize the 4S model. So, Fig. 8 (bottom-right) should be interpreted as the full parameter space of the four-site model projected into the $c_u - c_d$ plane. To simplify the visualization of this area, we have varied the vector coupling between the Z_2 boson and SM electrons, g^e_{2V}, within the allowed region of Fig. 2 for the sample scenarios: $z = 0.8$ and $M_{Z2} = 600$, 1000 and 2000 GeV. This setup should give a full representation of the parameter space, $M_{Z2} = 600$ GeV being the minimum allowed mass and $M_{Z2} = 2000$ GeV being close to the maximum value of the mass permitted by unitarity. The parameter space for these values of M_{Z2} and the respective $M_{Z1} = 0.8 \times M_{Z2}$ is presented in Fig. 8 (bottom-right) by colored lines (see caption). Whenever the colored line describing a given $M_{Z1,Z2}$ value for the 4S model crosses the black contour corresponding to the same mass value, that crossing point would give the experimental sensitivity to a $Z_{1,2}$ boson with that mass. Here, by experimental sensitivity we mean the maximal portion of the parameter space that could be probed at the present Tevatron (or the minimal c_d, c_u couplings). More in detail, the portion of the colored line beyond the aforementioned crossing point would represent the excluded region in the $c_u - c_d$ parameter space. To clarify the interpretation, let us consider the following examples. For $M_{Z_2} = 1000$ GeV and $M_{Z_1} = 800$ GeV (green lines), one can see that the parameter space for the Z_1 boson (solid green line) is greatly excluded in the region of the $c_u - c_d$ plane above the black contour line labeled by 800 GeV. Only a small portion of the $c_u - c_d$ parameter space is instead excluded for the Z_2 boson (dashed green line). The $c_{u,d}$ couplings are indeed bounded to be $c_{u,d} \leq 10^{-3}$, as one can see from the crossing point between the dashed green line and the black contour labeled by 1000 GeV. Since, the two extra gauge bosons would be simultaneously produced, from the discussed green lines one should deduce that the most restrictive bound on the $c_{u,d}$ couplings comes from the Z_1 boson. If not observed, the crossing point of the solid green line representing $M_{Z1} = 800$ GeV with the black contour at 800 GeV would give the bound: $c_{u,d} \leq 210^{-4}$. Consider now a second scenario: $M_{Z2} = 2000$ GeV and $M_{Z1} = 1600$ GeV. This is represented by blue lines. In this case, the Tevatron has no sensitivity at all to the two extra gauge bosons. The solid blue line representing $M_{Z1} = 1600$ GeV, in fact, never

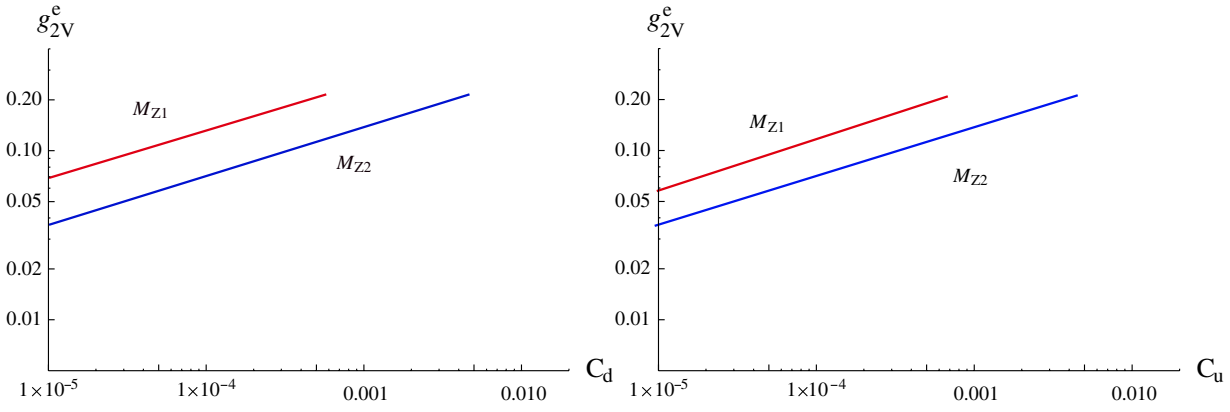

FIG. 9 (color online). g_{2v} fermion-boson coupling versus c_u (left) or c_d (right) in the four-site model.

crosses the corresponding black contour line labeled by 1600 GeV. And the same is true for the dashed blue line representing $M_{Z2} = 2000$ GeV.

Even in more complicated multiresonance scenarios, as in the 4S model, the $c_{u,d}$ representation allows one to visualize directly via the black contour lines, up to what mass value the experiment could be sensitive. If no signal of new physics is observed, the bound on the mass can be translated into limits on the $c_{u,d}$ coefficients. From there, one can then trace back exactly the Lagrangian parameters of the 4S model which are in turn excluded. In case of new physics discovery, the $c_{u,d}$ approach allows one to uniquely determine the $c_{u,d}$ values corresponding to that observed mass. Since the $c_{u,d}$ coefficients are strictly related to the new gauge boson couplings, this in turn enables one to extract informations on their size. In the 4S model, the coupling between the Z_2 boson and SM electrons, g^e_{2V}, grows linearly with c_u and c_d as shown in Fig. 9. Any mass measurement therefore translates into a coupling determination. Moreover, g^e_{2V} is one of the three free parameters of the model. The measurement of the mass of the new gauge bosons would therefore allow one to derive direct informations on the bare Lagrangian parameters.

B. Expected LHC potential at 7 TeV to probe Z' models

We now explore the LHC at 7 TeV potential to test the classes of Z' models under consideration. We use the projected limits from LHC. In particular, we rely on the limits given by the CMS Exotica Group for 500 pb^{-1} of integrated luminosity which hopefully will be available in about one year from now. This limit is shown in Fig. 10 (left panel), which is taken from the public Web page of the CMS Exotica Group [68]. The projected 500 pb^{-1} limit from CMS is given as a ratio $\sigma_{Z'}/\sigma_Z$, where σ_Z is the Z-boson production cross section in the $60 < m_{ee} < 120$ GeV window, and we have converted this limit into the limit on the NNLO production cross section for the Z' boson shown in terms of $c_{u,d}$ coefficients in $c_u - c_d$ plane for different Z' masses given in the right panel of Fig. 10. This representation is analogous to what has been done before at the Tevatron. Comparing Figs. 7 and 10, one can observe the strong gain in sensitivity one gets at the LHC at 7 TeV with 500 pb^{-1}, compared to the Tevatron with 5.4 fb^{-1}, at fixed $c_{u,d}$ value.

Now we can estimate the LHC at 7 TeV potential for deriving bounds on Z' models at 500 pb^{-1}. The results are shown in Fig. 11, where the legend scheme is the same as in Fig. 8. From Figs. 8 and 11, one can see that for the models with small-intermediate values of Z' boson couplings to SM fermions (that is E_6 models, GLR models partly, and some GSM models), the LHC at 7 TeV can extend the limits on $M_{Z'}$ by about 500 GeV when compared to the Tevatron. For example, the limit on the SM-like Z' boson could be extended from 1020 GeV to about 1520 GeV. On the other hand, the limits for larger $c_{u,d}$ coefficients and, respectively, larger masses could be extended in the near future up to a 2 TeV scale, which is unreachable at the Tevatron. For the Q model, belonging to the GSM class, the mass bound could be improved from 1210 GeV (current Tevatron) to 2250 GeV. Regarding the 4S model, one can see that the scenario characterized by $M_{Z1} = 800$ GeV and $M_{Z2} = 1000$ GeV could be totally excluded in the $c_u - c_d$ plane shown in Fig. 11. The solid green line, representing the Z_1 boson parameter space, lies in fact beyond the 800 GeV black contour line in the displayed plane. Like the Tevatron, the LHC will not

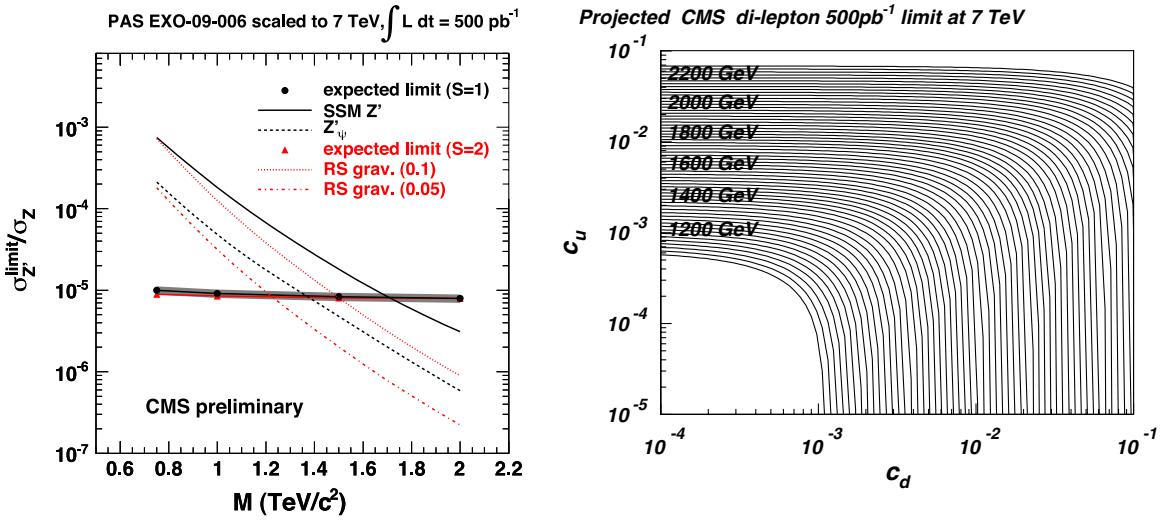

FIG. 10 (color online). Left: CMS limit on the Z' boson production cross section in the dielectron channel, normalized to the SM Z boson cross section, as a function of the Z' mass. The limit is projected at 500 pb^{-1} [68]. Right: Limits in the $c_u - c_d$ plane, based on the projected LHC 500 pb^{-1} limit shown in the right panel. In the $c_u - c_d$ representation, the limits appear as contour lines corresponding to different $M_{Z'}$ values.

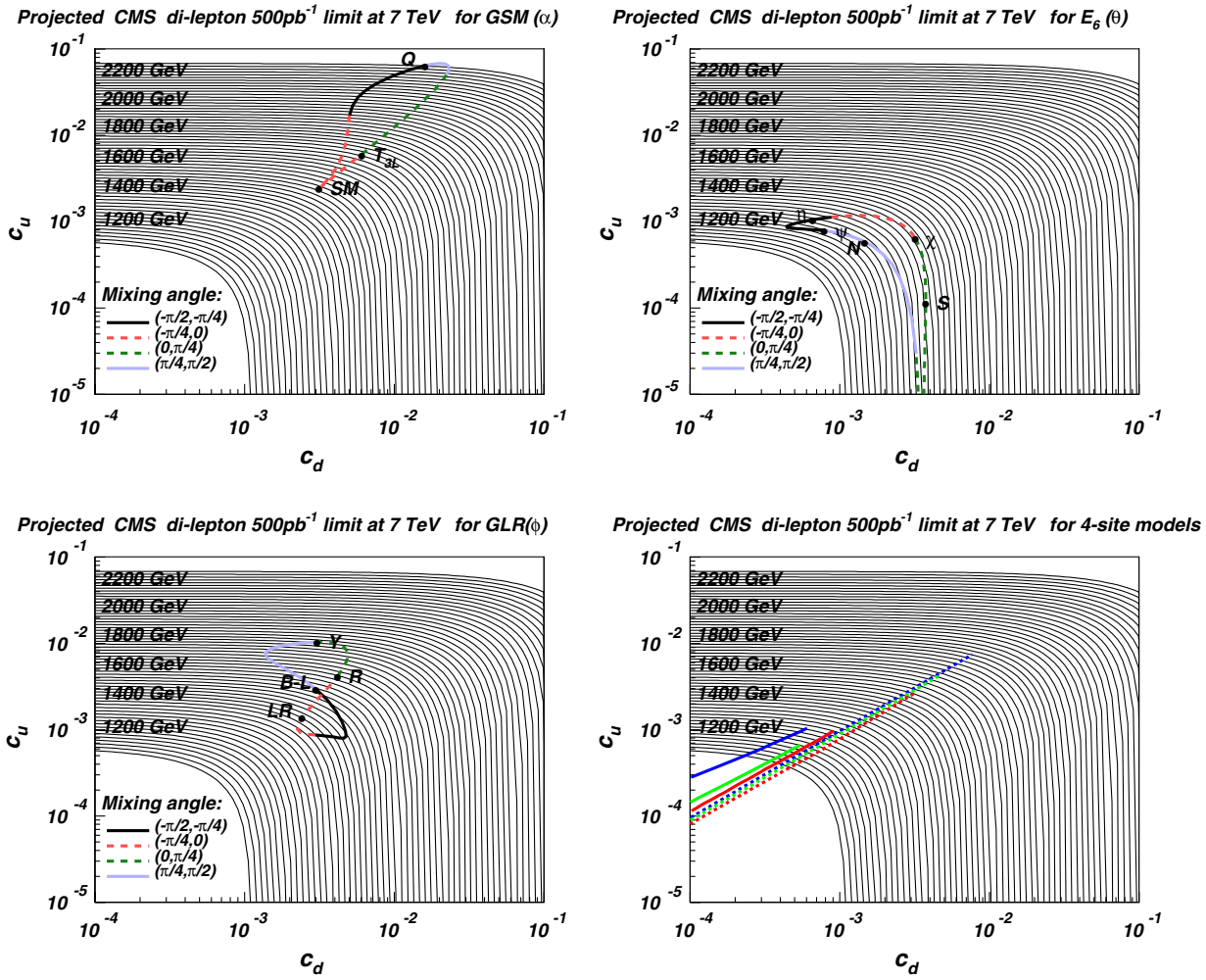

FIG. 11 (color online). Limits in $c_u - c_d$ plane are based on projected CMS 500 pb^{-1} limit. 95% C.L. limits on $M_{Z'}$ in the $c_u - c_d$ plane based on the projected CMS 500 pb^{-1} analysis of the dielectron channel. The legend scheme is the same as in Fig. 8.

able to test the scenario with $M_{Z_1} = 1600$ GeV and $M_{Z_2} = 2000$. The LHC at 7 TeV and 500 pb^{-1} will not have sensitivity enough, as one can deduce from observing that the blue lines never cross the black contour lines labeled by their respective mass values. Exploring this region of the 4S parameter space would require higher integrated luminosity and preferably higher collider energy.

We also use Fig. 10 to estimate the LHC at 7 TeV discovery limits for 500 pb^{-1}. In this analysis, we assume that the significance grows as $\sqrt{L}$, where L is the total integrated luminosity and the signal over background ratio is constant for the same selection cuts. The last assumption is motivated by the fact that for a chosen di-lepton invariant mass window the $q\bar{q}$ parton densities are very similar for signal and background processes and defined mainly by the the $\sqrt{s}$ value.

The LHC discovery potential for various Z' models is shown in Fig. 12 in the $c_u - c_d$ plane. The legend scheme is the same as in Fig. 8. The upper (dashed) and lower (dot-dashed) contours correspond to the uncertainty in Fig. 10 (left) reflected in the width of the band. One can see that discovery limits are typically 150–200 GeV lower than exclusion ones.

V. IMPACT OF THE Z' WIDTH ON SEARCH STRATEGIES

Invariant mass distributions may be examined in a number of ways for evidence of resonant structures. The sensitivity of any particular approach has a dependence on the intrinsic width of any possible resonance. The simplest approach is to bin the invariant mass distribution and determine the compatibility of the number of events in any bin with the standard model prediction. A p value may be used to quantify this compatibility. In this approach the width of the bins for optimal sensitivity depends on the intrinsic width of possible resonances and the detector resolution. In the case where the width of the resonance is much smaller than the detector resolution this parameter defines the optimal bin size. For intrinsic widths

comparable to the detector resolution, the optimal width depends on both of these parameters.

An alternative is to use a parameterization of the expected distribution in the two alternative hypotheses of, a distribution resulting only from standard model physics and one resulting from the addition of a new physics process. A comparison of some measure of the quality of the fit in both cases allows a determination of the probability of the presence of new physics. In this case the functional form of the resonance structure is typically taken to be some variant on a convolution of a Gaussian and a Breit-Wigner. For a resonance where the width of the Breit-Wigner is small in comparison to the width of the Gaussian the sensitivity of the search is insensitive to the width of the Breit-Wigner. Such circumstances result in the greatest possible experimental sensitivity. For resonances with large widths compared to the experimental resolution then the Breit-Wigner width must be included as a further parameter in any fits. In cases where the interference effect is large this must be included in the functional form used to fit to the invariant mass distribution. We show here that in the mass regions which will provide the greatest sensitivity for low integrated luminosities at the LHC the interference effect is negligible and may be ignored without compromising the search sensitivity.

The above descriptions of possible methods of searching for a resonance in an invariant mass distribution illustrate that a knowledge of the width of the resonances being searched for has an impact on the search procedure used. In order to obtain the best sensitivity, it is thus important to have a knowledge of the magnitude of the widths from new physics models. The results of such searches depend on the assumptions made in the analysis and cannot be easily interpreted in other circumstances.

Besides that, in the case of a discovery the Z' boson mass and decay width will be determined from fits to the

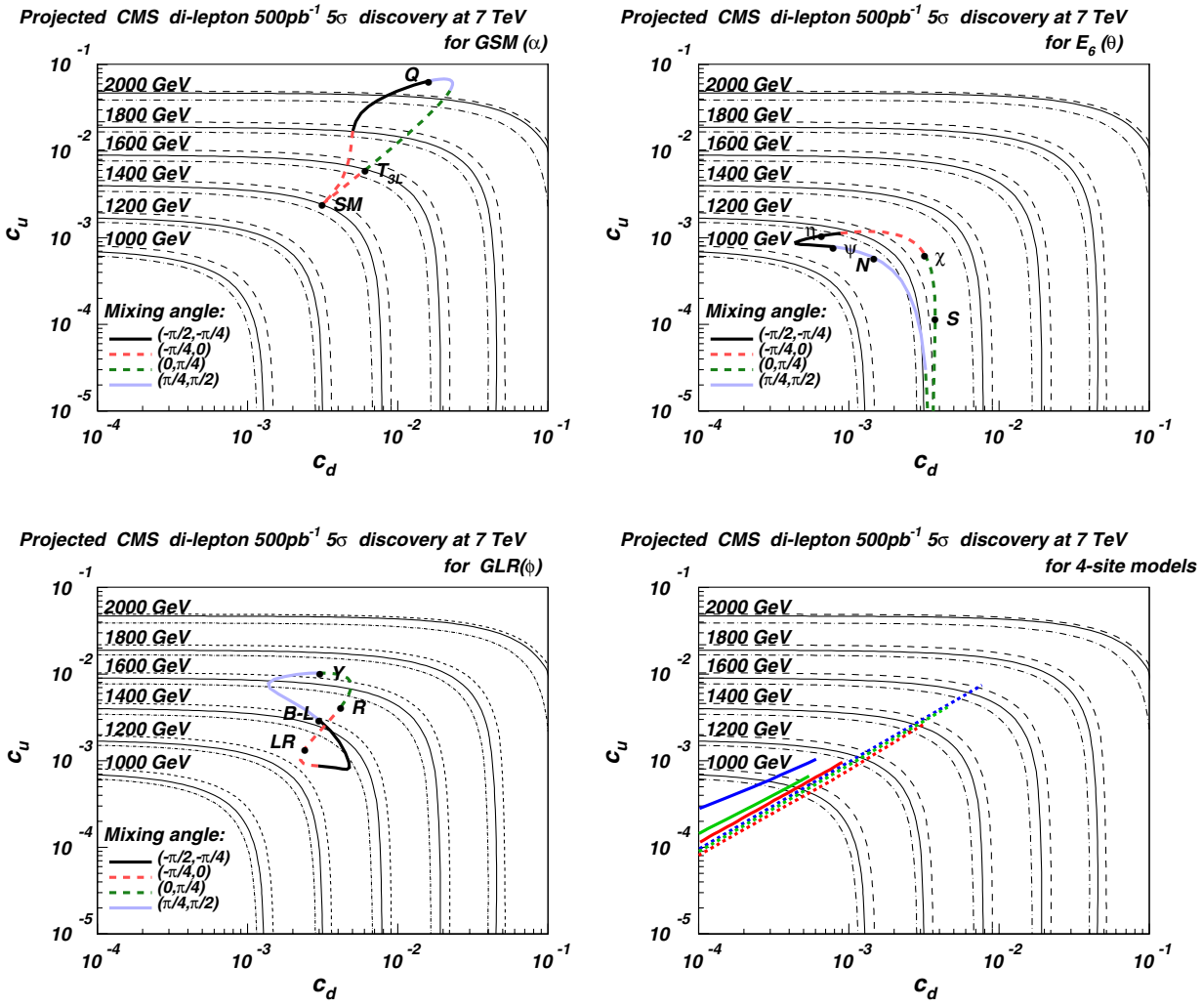

FIG. 12 (color online). 5σ discovery limits in the $c_u - c_d$ plane, based on the 500 pb^{-1} projected analysis of the Z' production in the dielectron channel performed by the CMS Collaboration. The legend scheme is the same as in Fig. 8. The upper (dashed) and lower (dot-dashed) contours correspond to the uncertainty in Fig. 10 (left) reflected in the width of the band.

reconstructed invariant mass distribution of dilepton candidate events. In this section, we thus focus on the prediction and the possible measurement of the total decay width, comparing the various classes of models under consideration.

All extra $U'(1)$ theories summarized in Table I make the assumption, for the sake of simplicity, that the Z' boson decays purely into SM fermions. Under this approximation, the total decay width is given by Eq. (3.6), and its value never exceeds a few percent of the corresponding mass ($\Gamma_{Z'}/M_{Z'} \leq 3\%$), as shown in Table II. This property has a direct implication on the possibility to measure the Z' decay width at the LHC, being correlated to the experimental dilepton mass resolution. If indeed $\Gamma_{Z'} \geq R$, being R the mass resolution, one can have direct access to the decay width of the observed spin-1 particle. During the early stage of the 7 TeV LHC, the expected dielectron mass resolution is about $R_{\mathrm{LHC}} = 2\% M_{Z'}$ [69,70]. As a consequence, within the majority of models summarized in Table II the total Z' boson width is hardly measurable. This is visualized in Fig. 13, where the ratio between Z' width and mass is plotted as a function of the mixing angle parametrizing the three classes of models listed in Table I: E_6, GLR, and GSM. All E_6 inspired models predict a quite narrow Z' boson. For some benchmark models within the GLR), the ratio becomes slightly bigger than the early LHC resolution. The scenario changes when we consider GSMs. Here, the width over mass ratio is well above the early 2% resolution of the LHC. Another example of measurable decay width is given by the four-site Higgsless model. Here, in fact, in most of the parameter space $\Gamma_{Z_{1,2}}/M_{Z_{1,2}} \geq 2\%$. This property is shown in Fig. 14 for different values of the free z parameter. In this case, the distinctive behavior is due to the fact that the $Z_{1,2}$ bosons predicted by the four-site model decay preferably into the diboson channel: $Z_1 \rightarrow WW$ and $Z_2 \rightarrow W_1 W$. Thus, their width grows with the third power of the corresponding mass, as shown in Eqs. (3.11) and (3.12), making it wider compared to the other models. This feature is common to all Higgsless and Technicolor models.

This discussion is appropriate when considering the Z' boson production in the dielectron Drell-Yan channel. For dimuon final states, the analysis would change drastically. The estimated dimuon mass resolution during the early stage of the 7 TeV LHC is in fact around $R \simeq 8\%$ [69,70]. Hence, only in a very restricted range of the

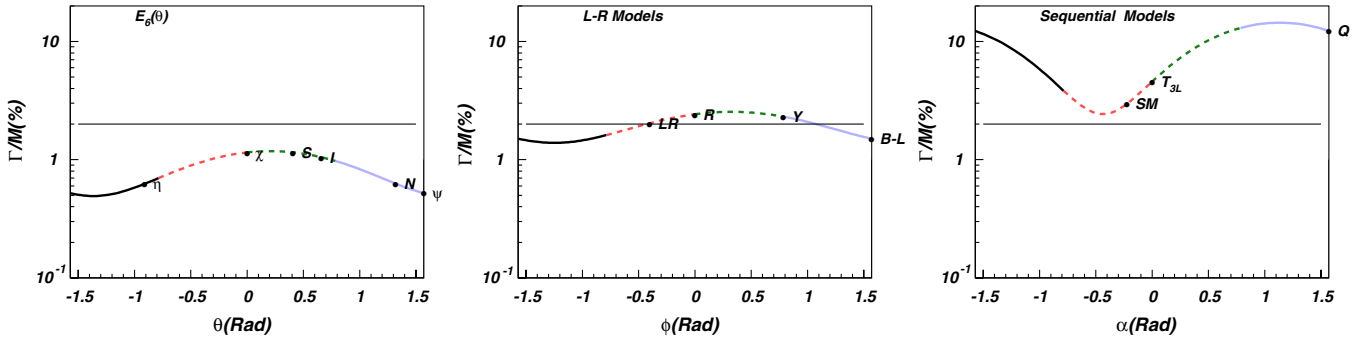

FIG. 13 (color online). Z' boson width over its mass as a function of the mixing angle parametrizing the E_6, GLR, and GSM classes of models given in Table I. The color code corresponds to four equidistant intervals in the $[-\pi/2, \pi/2]$ region. The black dots on the contours correspond to the benchmark models listed in Table I.

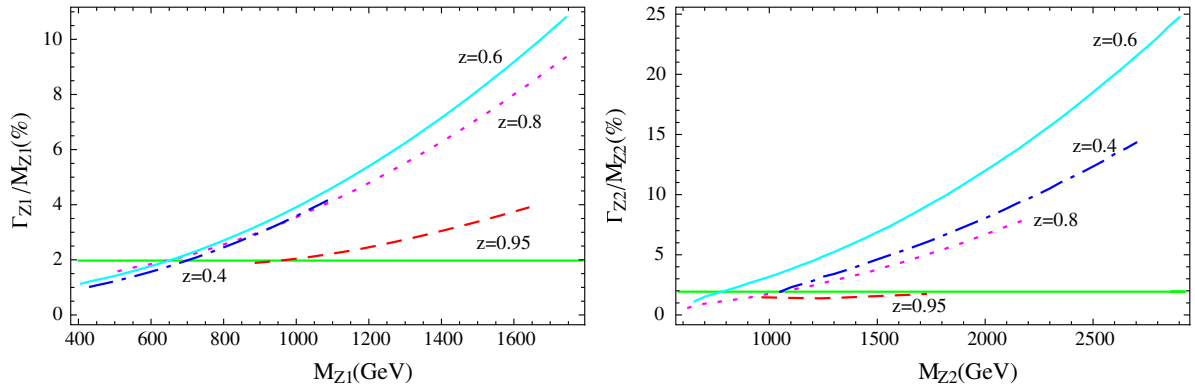

FIG. 14 (color online). Left: Z_1 boson width over its mass as a function of M_{Z1} for different values of the free z parameter. Right: same for the Z_2 boson. We assume the maximal Z_2-boson coupling to SM fermions.

GSM mixing angle the Z' width could be measurable. An exception is given by the four-site Higgsless model, where the Z_2 boson width could be determined in a large portion of the parameter space.

The discussed differences between classes of models should be taken into account for improving search strategies and possibly measurements.

VI. SUMMARY AND CONCLUSIONS

In this paper we have discussed the prospects for setting limits on or discovering spin-1 Z' bosons using early LHC data at 7 TeV. In order to facilitate the connection between experimental data and theoretical models, we have advocated the narrow width approximation, in which the leptonic Drell-Yan Z' boson production cross section only depends on the Z' boson mass together with two parameters, c_u and c_d. These variables provide a convenient way of expressing the experimental limits or discovery information about the mass and cross section, which enables a direct comparison to be made with the predictions arising from theoretical models. The experimental limits on the Z' boson cross section may be expressed as contours in the $c_u - c_d$ plane, with a unique contour for each value of Z' boson mass. If a discovery is made, then the measurement of the mass and cross section would correspond to some unique contour, or in practice a unique band including the experimental uncertainty. Such contours may be compared to the theoretical prediction of c_u and c_d arising from particular models, enabling limits to be set on models or a discovery to discriminate between particular models. However, the application of this strategy requires the experimental cross sections to be properly defined and the theoretical cross sections to be accurately calculated, as we now discuss.

On the experimental side, we have seen that the use of the narrow width approximation requires an appropriate dilepton invariant mass window cut around the mass of the Z' boson. The effect of the cuts is rather subtle, since it depends on both the width of the Z' boson and the energy of the collider, with higher widths and lower collider energies leading to more prominent signal tails at low invariant masses. Fortunately we have seen that at LHC energies the suitable experimental cut is rather insensitive, especially for models with lower Z' boson widths, and furthermore may be optimized at a unique value suitable for all models, although there is some unavoidable dependence on the Z' mass. One important conclusion is that whatever cut is chosen should involve invariant masses well above 100 GeV, otherwise interference effects will be dominant. In summary, we have demonstrated that this cut plays a crucial role: it diminishes a possibly huge model-dependent interference effect, removes the model-dependent shape of the $M_{\ell^+\ell^-}$ distributions in the region of low $M_{\ell^+\ell^-}$, especially for the case of large Z' width, and brings into agreement NWA and exact cross sections. On the theoretical side, we have evaluated cross sections at NNLO using the updated ZWPROD package. One should stress that K_{NNLO} factors are depend on the Z' mass, and we have tabulated them for convenience for both the Tevatron and LHC. Moreover, the K_{NNLO} are very PDF dependent, and one should specify which PDF is being used to apply a respective K_{NNLO}.

We have applied the approach above to two quite different types of Z' models: perturbative gauge models and strongly coupled models. Among the perturbative gauge models, we have studied three classes: E_6 models, left-right symmetric models, and sequential standard models. Each class of model is defined in terms of a continuous mixing angle variable. This enabled infinite classes of benchmark models to be defined, rather than just a finite number of models, where for each class of model, the respective angles serve to parametrize different orbits in the $c_u - c_d$ plane. These orbits turn out to be nonoverlapping for these three classes of models.

The set of perturbative models under study was restricted for the sake of simplicity and does not include examples with the effect of non-SM particles (and right-handed neutrinos) on the width $\Gamma_{Z'}$. Assuming only SM particles in the final state, we have calculated the widths of the benchmark classes of models and seen that the perturbative models generally involve relatively narrow widths (which however can be increased if non-SM particles are included in the decays), while the strongly coupled models involve multiple Z' bosons with rather broad widths. We have also commented on the significance of the width on search strategies, which if measured, would provide complementary information for the discrimination of the underlying Z' model as well as allowing to test the non-SM Z' decays mentioned above. Another limitation of the choice of models under study is that they do not include the effects of $Z - Z'$ mixing, which is quite model dependent. However, such effects must be small due to the constraints from electroweak precision measurements, so such effects will not have a major effect on the direct collider searches considered here, although of course they will affect the precise vector and axial couplings (see for example [6–8] where the $U(1)_N$ vector and axial vector couplings are calculated including the mixing effects). Regarding strongly coupled models, we only considered the four-site Higgsless model which contains just two excitations of the Z (and W) bosons. However, it is representative of models of walking technicolor models and the KK excitations of the Z (and W), which is considered for the first time in the $c_u - c_d$ plane. It is clearly seen that the associated Z' bosons may easily be distinguished from those of the perturbative gauge models.

In conclusion, our results support the use of the narrow width approximation in which the leptonic Drell-Yan Z' boson production cross section only depends on the Z' boson mass together with two parameters c_u and c_d.

However, as discussed in this paper, care must be taken concerning the experimental cuts, and the theoretical K_{NNLO} factors tabulated here must be included correctly. Providing the experimental cross section is appropriately defined, according to the method we provide in Fig. 6, and the theoretical cross sections are properly calculated at NNLO, we have shown that such a strategy is safe, convenient and provides the most unbiased way of comparing experiment to theoretical models which avoids any built-in model-dependent assumptions. The experimental limits or discovery bands may then be reliably confronted with the theoretical predictions on the $c_u - c_d$ plane as shown in Figs. 8, 11, and 12, which represent the main results of our study, leading to the new limits which we derive here for the Tevatron and to the projected limits for the LHC. The results show that the LHC at 7 TeV with as little data as 500 pb^{-1} can either greatly improve on current Tevatron mass limits, or discover a Z', with a measurement of the mass and cross section providing a powerful discriminator between the benchmark models using this approach.

ACKNOWLEDGMENTS

We would like to thank P. Nadolsky, A. Pukhov, D. Ross, and I. Tomalin for stimulating discussions. A. B. and S. K. would like to thank C. Hays and S. Harper for help with understanding the details of the experimental analysis at CDF and CMS. A. B. would like to acknowledge the support of the International Joint Project Royal Society under Grant No. JP090598. L. F. would like to thank the School of Physics & Astronomy of the University of Southampton for hospitality.

APPENDIX: K_{NNLO} FACTORS AND CROSS SECTIONS FOR THE $p\bar{p}(p) \to Z' + X$ PRODUCTION PROCESS AT THE TEVATRON AND THE LHC AT 7 TEV

TABLE III. Values of K_{NNLO} factors and cross sections for the $p\bar{p}(p) \to Z' + X$ production process at the Tevatron and the LHC at 7 TeV, obtained with the ZWPROD package for MSTW08 PDF.

$M_{Z'}$ (GeV)	Tevatron			LHC at 7 TeV		
	σ_{LO} (pb)	σ_{NNLO} (pb)	K_{NNLO}	σ_{LO} (pb)	σ_{NNLO} (pb)	K_{NNLO}
100	3.96×10^3	5.57×10^3	1.41	1.63×10^4	2.12×10^4	1.29
150	1.08×10^3	1.56×10^3	1.44	4.45×10^3	5.87×10^3	1.32
200	4.15×10^2	6.09×10^2	1.47	1.70×10^3	2.28×10^3	1.34
250	1.90×10^2	2.83×10^2	1.49	7.89×10^2	1.06×10^3	1.35
300	9.67×10	1.45×10^2	1.50	4.14×10^2	5.60×10^2	1.35
350	5.25×10	7.91×10	1.51	2.37×10^2	3.20×10^2	1.35
400	2.96×10	4.49×10	1.51	1.44×10^2	1.95×10^2	1.35
450	1.72×10	2.61×10	1.52	9.20×10	1.24×10^2	1.35
500	1.02×10	1.54×10	1.52	6.10×10	8.22×10	1.35
550	6.05	9.20	1.52	4.16×10	5.60×10	1.34
600	3.62	5.51	1.52	2.92×10	3.91×10	1.34
650	2.17	3.30	1.52	2.08×10	2.79×10	1.34
700	1.29	1.97	1.52	1.52×10	2.02×10	1.33
750	7.68×10^{-1}	1.16	1.52	1.12×10	1.49×10	1.33
800	4.52×10^{-1}	6.83×10^{-1}	1.51	8.35	1.11×10	1.32
850	2.63×10^{-1}	3.97×10^{-1}	1.51	6.30	8.32	1.32
900	1.51×10^{-1}	2.28×10^{-1}	1.51	4.80	6.32	1.32
950	8.52×10^{-2}	1.28×10^{-1}	1.50	3.69	4.84	1.31
1000	4.72×10^{-2}	7.11×10^{-2}	1.51	2.86	3.73	1.31
1050	2.56×10^{-2}	3.85×10^{-2}	1.50	2.23	2.90	1.30
1100	1.35×10^{-2}	2.03×10^{-2}	1.50	1.74	2.26	1.30
1150	6.95×10^{-3}	1.04×10^{-2}	1.50	1.37	1.78	1.29
1200	3.45×10^{-3}	5.20×10^{-3}	1.51	1.09	1.40	1.29
1250	1.65×10^{-3}	2.49×10^{-3}	1.51	8.63×10^{-1}	1.11	1.29
1300	7.52×10^{-4}	1.14×10^{-3}	1.52	6.88×10^{-1}	8.82×10^{-1}	1.28
1350	3.25×10^{-4}	4.95×10^{-4}	1.52	5.50×10^{-1}	7.03×10^{-1}	1.28
1400	1.32×10^{-4}	2.02×10^{-4}	1.53	4.41×10^{-1}	5.63×10^{-1}	1.28

TABLE III. (*Continued*)

$M_{Z'}$ (GeV)	Tevatron			LHC at 7 TeV		
1450	4.97×10^{-5}	7.66×10^{-5}	1.54	3.55×10^{-1}	4.51×10^{-1}	1.27
1500	1.71×10^{-5}	2.65×10^{-5}	1.55	2.86×10^{-1}	3.63×10^{-1}	1.27
1550				2.31×10^{-1}	2.92×10^{-1}	1.27
1600				1.87×10^{-1}	2.36×10^{-1}	1.26
1650				1.52×10^{-1}	1.91×10^{-1}	1.26
1700				1.23×10^{-1}	1.55×10^{-1}	1.26
1750				1.00×10^{-1}	1.26×10^{-1}	1.25
1800				8.17×10^{-2}	1.02×10^{-1}	1.25
1850				6.67×10^{-2}	8.31×10^{-2}	1.25
1900				5.44×10^{-2}	6.78×10^{-2}	1.25
1950				4.45×10^{-2}	5.53×10^{-2}	1.24
2000				3.64×10^{-2}	4.51×10^{-2}	1.24
2050				2.98×10^{-2}	3.69×10^{-2}	1.24
2100				2.44×10^{-2}	3.02×10^{-2}	1.24
2150				2.00×10^{-2}	2.47×10^{-2}	1.23
2200				1.64×10^{-2}	2.02×10^{-2}	1.23
2250				1.34×10^{-2}	1.65×10^{-2}	1.23
2300				1.10×10^{-2}	1.35×10^{-2}	1.23
2350				9.04×10^{-3}	1.11×10^{-2}	1.23
2400				7.41×10^{-3}	9.08×10^{-3}	1.23
2450				6.08×10^{-3}	7.44×10^{-3}	1.22
2500				4.98×10^{-3}	6.09×10^{-3}	1.22

TABLE IV. Values of K_{NNLO} factors and cross sections for the $p\bar{p}(p) \to Z' + X$ production process at the Tevatron and the LHC at 7 TeV, obtained with the ZWPROD package for CTEQ6.6 PDF.

$M_{Z'}$ (GeV)	Tevatron			LHC at 7 TeV		
	σ_{LO} (pb)	σ_{NNLO} (pb)	K_{NNLO}	σ_{LO} (pb)	σ_{NNLO} (pb)	K_{NNLO}
100	3.94×10^{3}	5.40×10^{3}	1.37	1.52×10^{4}	1.95×10^{4}	1.28
150	1.12×10^{3}	1.54×10^{3}	1.37	4.23×10^{3}	5.46×10^{3}	1.29
200	4.47×10^{2}	6.08×10^{2}	1.36	1.64×10^{3}	2.13×10^{3}	1.30
250	2.12×10^{2}	2.85×10^{2}	1.34	7.66×10^{2}	1.00×10^{3}	1.31
300	1.11×10	1.47×10^{2}	1.32	4.04×10^{2}	5.29×10^{2}	1.31
350	6.14×10	8.03×10	1.31	2.32×10^{2}	3.04×10^{2}	1.31
400	3.54×10	4.57×10	1.29	1.42×10^{2}	1.85×10^{2}	1.31
450	2.10×10	2.67×10	1.27	9.08×10	1.18×10^{2}	1.30
500	1.26×10	1.58×10	1.26	6.04×10	7.85×10	1.30
550	7.61	9.46	1.24	4.13×10	5.35×10	1.29
600	4.63	5.68	1.23	2.90×10	3.74×10	1.29
650	2.81	3.42	1.21	2.08×10	2.67×10	1.28
700	1.70	2.05	1.20	1.51×10	1.94×10	1.28
750	1.03×10^{-1}	1.22	1.19	1.12×10	1.42×10	1.27
800	6.12×10^{-1}	7.21×10^{-1}	1.18	8.38	1.06×10	1.26
850	3.61×10^{-1}	4.22×10^{-1}	1.17	6.35	7.98	1.26
900	2.11×10^{-1}	2.44×10^{-1}	1.16	4.85	6.06	1.25
950	1.21×10^{-2}	1.39×10^{-1}	1.15	3.74	4.64	1.24
1000	6.80×10^{-2}	7.77×10^{-2}	1.14	2.90	3.59	1.24
1050	3.75×10^{-2}	4.26×10^{-2}	1.13	2.27	2.78	1.23
1100	2.02×10^{-2}	2.28×10^{-2}	1.13	1.78	2.18	1.22
1150	1.06×10^{-3}	1.19×10^{-2}	1.13	1.41	1.71	1.21
1200	5.36×10^{-3}	6.04×10^{-3}	1.13	1.12	1.35	1.21
1250	2.62×10^{-3}	2.96×10^{-3}	1.13	8.88×10^{-1}	1.07	1.20
1300	1.23×10^{-3}	1.39×10^{-3}	1.13	7.10×10^{-1}	8.48×10^{-1}	1.19
1350	5.49×10^{-4}	6.24×10^{-4}	1.14	5.70×10^{-1}	6.77×10^{-1}	1.19

TABLE IV. (*Continued*)

$M_{Z'}$ (GeV)	Tevatron			LHC at 7 TeV		
	σ_{LO} (pb)	σ_{NNLO} (pb)	K_{NNLO}	σ_{LO} (pb)	σ_{NNLO} (pb)	K_{NNLO}
1400	2.31×10^{-4}	2.65×10^{-4}	1.15	4.58×10^{-1}	5.42×10^{-1}	1.18
1450	9.08×10^{-5}	1.05×10^{-5}	1.16	3.70×10^{-1}	4.35×10^{-1}	1.18
1500	3.28×10^{-5}	3.86×10^{-5}	1.18	2.99×10^{-1}	3.50×10^{-1}	1.17
1550				2.42×10^{-1}	2.82×10^{-1}	1.16
1600				1.97×10^{-1}	2.28×10^{-1}	1.16
1650				1.60×10^{-1}	1.85×10^{-1}	1.15
1700				1.31×10^{-1}	1.50×10^{-1}	1.15
1750				1.06×10^{-1}	1.22×10^{-1}	1.14
1800				8.70×10^{-2}	9.92×10^{-1}	1.14
1850				7.12×10^{-2}	8.09×10^{-2}	1.14
1900				5.83×10^{-2}	6.60×10^{-2}	1.13
1950				4.77×10^{-2}	5.40×10^{-2}	1.13
2000				3.92×10^{-2}	4.41×10^{-2}	1.13
2050				3.21×10^{-2}	3.61×10^{-2}	1.13
2100				2.64×10^{-2}	2.96×10^{-2}	1.12
2150				2.17×10^{-2}	2.43×10^{-2}	1.12
2200				1.78×10^{-2}	2.00×10^{-2}	1.12
2250				1.46×10^{-2}	1.64×10^{-2}	1.12
2300				1.20×10^{-2}	1.35×10^{-2}	1.12
2350				9.88×10^{-3}	1.11×10^{-2}	1.12
2400				8.12×10^{-3}	9.10×10^{-3}	1.12
2450				6.67×10^{-3}	7.48×10^{-3}	1.12
2500				5.48×10^{-3}	6.15×10^{-3}	1.12

[1] P. Langacker, Rev. Mod. Phys. **81**, 1199 (2009).
[2] J. Erler, P. Langacker, S. Munir, and E. R. Pena, J. High Energy Phys. 08 (2009) 017.
[3] P. Nath *et al.*, Nucl. Phys. B, Proc. Suppl. **200-202**, 185 (2010).
[4] M. S. Carena, A. Daleo, B. A. Dobrescu, and T. M. P. Tait, Phys. Rev. D **70**, 093009 (2004).
[5] See M.-C. Chen and B. Dobrescu on pp. 446-450 of "The Review of Particle Physics" (2008), http://www.lorentz.leidenuniv.nl/research/neerven/DECEASED/Welcome.html; citation of the entire review: C. Amsler *et al.* (Particle Data Group) Phys. Lett. B **667**, 1 (2008).
[6] S. King, S. Moretti, and R. Nevzorov, Phys. Rev. D **73**, 035009 (2006).
[7] S. King, S. Moretti, and R. Nevzorov, Phys. Lett. B **634**, 278 (2006).
[8] R. Howl and S. King, J. High Energy Phys. 01 (2008) 030.
[9] Y. Li, F. Petriello, and S. Quackenbush, Phys. Rev. D **80**, 055018 (2009).
[10] R. Diener, S. Godfrey, and T. A. Martin, arXiv:1006.2845.
[11] J. Erler, P. Langacker *et al.* (, and , arXiv:1010.3097.
[12] F. Petriello and S. Quackenbush, Phys. Rev. D **77**, 115004 (2008).
[13] E. Accomando, S. De Curtis, D. Dominici, and L. Fedeli, Phys. Rev. D **83**, 015012 (2011).
[14] L. Basso, S. Moretti, and G. M. Pruna, arXiv:1009.4164.
[15] L. Basso, A. Belyaev, S. Moretti, G. M. Pruna, and C. H. Shepherd-Themistocleous, arXiv:1002.3586.
[16] P. Athron, S. King, D. J. Miller, S. Moretti, and R. Nevzorov *et al.*, Phys. Lett. B **681**, 448 (2009).
[17] P. Athron, S. King, D. Miller, S. Moretti, and R. Nevzorov, Phys. Rev. D **80**, 035009 (2009).
[18] T. Appelquist, B. A. Dobrescu, and A. R. Hopper, Phys. Rev. D **68**, 035012 (2003).
[19] C. P. Hays, A. V. Kotwal, and O. Stelzer-Chilton, Mod. Phys. Lett. A **24**, 2387 (2009).
[20] E. Salvioni, G. Villadoro, and F. Zwirner, J. High Energy Phys. 11 (2009) 068.
[21] E. Salvioni, A. Strumia, G. Villadoro, and F. Zwirner, J. High Energy Phys. 03 (2010) 010.
[22] R. Casalbuoni, S. De Curtis, D. Dominici, and R. Gatto, Phys. Lett. B **155**, 95 (1985).
[23] D. London and J. L. Rosner, Phys. Rev. D **34**, 1530 (1986).
[24] J. Kang and P. Langacker, Phys. Rev. D **71**, 035014 (2005).
[25] R. Foadi, M. T. Frandsen, T. A. Ryttov, and F. Sannino, Phys. Rev. D **76**, 055005 (2007).
[26] A. Belyaev *et al.*, Phys. Rev. D **79**, 035006 (2009).
[27] E. Accomando, S. De Curtis, D. Dominici, and L. Fedeli, Phys. Rev. D **79**, 055020 (2009).
[28] E. Accomando, S. De Curtis, D. Dominici, and L. Fedeli, Nuovo Cimento Soc. Ital. Fis. B **123**, 809 (2008).
[29] R. Sekhar Chivukula, D. A. Dicus, and H.-J. He, Phys. Lett. B **525**, 175 (2002).
[30] C. Csaki, C. Grojean, H. Murayama, L. Pilo, and J. Terning, Phys. Rev. D **69**, 055006 (2004).
[31] K. Agashe, A. Delgado, M. J. May, and R. Sundrum, J. High Energy Phys. 08 (2003) 050.
[32] C. Csaki, C. Grojean, L. Pilo, and J. Terning, Phys. Rev. Lett. **92**, 101802 (2004).

[33] R. Barbieri, A. Pomarol, and R. Rattazzi, Phys. Lett. B **591**, 141 (2004).
[34] Y. Nomura, J. High Energy Phys. 11 (2003) 050.
[35] G. Cacciapaglia, C. Csaki, C. Grojean, and J. Terning, in *The 32nd SLAC Summer Institute on Particle Physics Nature's Greatest Puzzles*, 2–13 August 2004, Menlo Park, California econf C040802, FRT004 (2004).
[36] G. Cacciapaglia, C. Csaki, C. Grojean, and J. Terning, Phys. Rev. D **71**, 035015 (2005).
[37] G. Cacciapaglia, C. Csaki, C. Grojean, and J. Terning, Phys. Rev. D **70**, 075014 (2004).
[38] R. Contino, T. Kramer, M. Son, and R. Sundrum, J. High Energy Phys. 05 (2007) 074.
[39] R. Casalbuoni, S. De Curtis, D. Dolce, and D. Dominici, Phys. Rev. D **71**, 075015 (2005).
[40] N. Arkani-Hamed, A. G. Cohen, and H. Georgi, Phys. Rev. Lett. **86**, 4757 (2001).
[41] N. Arkani-Hamed, A. G. Cohen, and H. Georgi, Phys. Lett. B **513**, 232 (2001).
[42] C. T. Hill, S. Pokorski, and J. Wang, Phys. Rev. D **64**, 105005 (2001).
[43] H.-C. Cheng, C. T. Hill, S. Pokorski, and J. Wang, Phys. Rev. D **64**, 065007 (2001).
[44] H. Abe, T. Kobayashi, N. Maru, and K. Yoshioka, Phys. Rev. D **67**, 045019 (2003).
[45] A. Falkowski and H. D. Kim, J. High Energy Phys. 08 (2002) 052.
[46] L. Randall, Y. Shadmi, and N. Weiner, J. High Energy Phys. 01 (2003) 055.
[47] D. T. Son and M. A. Stephanov, Phys. Rev. D **69**, 065020 (2004).
[48] J. de Blas, A. Falkowski, M. Perez-Victoria, and S. Pokorski, J. High Energy Phys. 08 (2006) 061.
[49] R. Casalbuoni, S. De Curtis, D. Dominici, and R. Gatto, Nucl. Phys. **B282**, 235 (1987).
[50] A. Birkedal, K. Matchev, and M. Perelstein, Phys. Rev. Lett. **94**, 191803 (2005).
[51] A. Belyaev, arXiv:0711.1919.
[52] H.-J. He *et al.*, Phys. Rev. D **78**, 031701 (2008).
[53] R. Barbieri, A. Pomarol, R. Rattazzi, and A. Strumia, Nucl. Phys. **B703**, 127 (2004).
[54] R. Hamberg, W. L. van Neerven, and T. Matsuura, Nucl. Phys. **B359**, 343 (1991).
[55] W. L. van Neerven and E. B. Zijlstra, Nucl. Phys. **B382**, 11 (1992).
[56] R. Hamberg, T. Matsuura, and W. van Neerven, ZWPROD program (1989–2002), http://www.lorentz.leidenuniv.nl/research/neerven/deceased/Welcome.html.
[57] C. Coriano, A. E. Faraggi, and M. Guzzi, Nuovo Cimento Soc. Ital. Fis. B **123**, 781 (2008).
[58] B. Fuks, arXiv:0805.2004.
[59] B. Fuks, M. Klasen, F. Ledroit, Q. Li, and J. Morel, Nucl. Phys. **B797**, 322 (2008).
[60] S. Kretzer, H. L. Lai, F. I. Olness, and W. K. Tung, Phys. Rev. D **69**, 114005 (2004).
[61] P. M. Nadolsky *et al.*, Phys. Rev. D **78**, 013004 (2008).
[62] A. D. Martin, W. J. Stirling, R. S. Thorne, and G. Watt, Eur. Phys. J. C **63**, 189 (2009).
[63] H.-L. Lai *et al.*, J. High Energy Phys. 04 (2010) 035.
[64] S. G. Gorishnii, A. L. Kataev, and S. A. Larin, Phys. Lett. B **212**, 238 (1988).
[65] A. L. Kataev, Phys. Lett. B **287**, 209 (1992).
[66] H. Chris, in *ICHEP 2010, Paris, France (2010)* (unpublished).
[67] V. M. Abazov *et al.* (D0 Collaboration), Phys. Lett. B **695**, 88 (2011).
[68] CMS Collaboration and Exotica Group, https://twiki.cern.ch/twiki/bin/view/CMS/HEEP7TeVscaled.
[69] G. L. Bayatian *et al.* (CMS Collaboration), CERN Report No. CERN-LHCC-2006-001 (unpublished).
[70] A. Airapetian *et al.* (ATLAS Collaboration), CERN Report No. CERN-LHCC-99-14 ATLAS, 1999.
[71] D. Feldman, Z. Liu, and P. Nath, Phys. Rev. Lett. **97**, 021801 (2006).
[72] D. Feldman, Z. Liu, and P. Nath, J. High Energy Phys. 11, (2006) 007.